Article

A New PID Controller Design with Constraints on Relative Delay Margin for First-Order Plus Dead-Time Systems

Zhenlong Wu, Donghai Li * and Yali Xue

State Key Lab of Power Systems, Department of Energy and Power Engineering, Tsinghua University, Beijing 100084, China; wu-zl15@mails.tsinghua.edu.cn (Z.W.); xueyali@mail.tsinghua.edu.cn (Y.X.)

* Correspondence: lidongh@mail.tsinghua.edu.cn; Tel.: +86-106-2782-772

check for updates

Abstract: The maximum sensitivity function as the conventional robustness index is often used to test the robustness and cannot be used to tune the controller parameters directly. To reduce analytical difficulties in dealing with the maximum sensitivity function and improve the control performance of the proportional-integral-derivative controller, the relative delay margin as a good alternative is proposed to offer a simple robust analysis for the proportional-integral-derivative controller and the first-order plus dead-time systems. The relationship between the parameters of the proportional-integral-derivative controller and the new pair, e.g., the phase margin and the corresponding gain crossover frequency, is derived. Based on this work, the stability regions of the proportional-integral-derivative controller parameters, the proportional gain and the integral gain with a given derivative gain, are obtained in a simple way. The tuning of the proportional-integral-derivative controller with constraints on the relative delay margin is simplified into an optimal disturbance rejection problem and the tuning procedure is summarized. For convenience, the recommended parameters are also offered. Simulation results demonstrate that the proposed methodology has better tracking and disturbance rejection performance than other comparative design methodologies of the proportional-integral/proportional-integral-derivative controller. For example, the integrated absolute errors of the proposed proportional-integral-derivative controller for the tracking performance and disturbance rejection performance are less than 91.3% and 91.7% of the integrated absolute errors of other comparative controllers in Example 3, respectively. The proposed methodology shows great potential in industrial applications. Besides, the proposed method can be applied to the design of the proportional-integral-derivative controller with filtered derivative which is recommended for practical applications to weaken the adverse influence of the high-frequency measurement noise.

Keywords: proportional-integral-derivative controller; relative delay margin; stability regions; desired robustness-constrained optimization

1. Introduction

The proportional-integral (PI)/proportional-integral-derivative (PID) controller plays a non-substitutable role and is widely used in industrial processes currently even though the advanced control theory has developed flourishingly [1]. These advanced control strategies, such as active disturbance rejection control [2], model predictive control [3], and slide model control [4], obtain the satisfactory control performance in simulations while they are rarely applied to practical applications.

The PI/PID controller is a simple feedback structure of the form "present-past-future", which does not depend on the precise mathematical models of the dynamical systems [5]. How to obtain the desired parameters of the PI/PID controller has been the concern of many researchers for a long

time [6]. Specifically, the research of the PI/PID controller tuning rules can date back to the work by Ziegler and Nicholas in 1942 [7]. The Ziegler and Nicholas (Z-N) method, lacking of the robustness constraint, needs the information of the gain margin and the associated frequency which is obtained by experiments on the process with some empirical rules [8]. A dual-point tuning method for the PI/PID controller is proposed by Åström and Hägglund which needs the gain margin (g_m) and the phase margin (φ_m) [9]. To better balance the control performance and robustness, the gain and phase margins are often set as $6 \leq g_m \leq 12$ dB and $30° \leq \varphi_m \leq 60°$ [10], and these margins have been widely used. However, the constraints are often used to test the robustness and cannot be used to design the controller directly. The maximum sensitivity function, M_s, is developed to be a good single robustness measure, and the integral gain is also found to be a good performance index for the disturbance rejection [11]. Many tuning rules are summarized in the handbook for different processes [12], such as M_s-constrained integral gain optimization (MIGO) [13] and Skogestad internal model control (SIMC) [6]. Recently, the generalized frequency method is proposed for a two-degree-of-freedom PID controller [14]. The tuning rules based on the desired closed-loop response [15], the linear quadratic regulator (LQR) [16] and the probabilistic robustness (PR) [17] are also developed for the PI/PID controller. Some new PID controller synthesis approaches are reported recently [18–21]. In [18], a PID controller is designed based on the optimal H_2 minimization framework for integrating and double integrating time delay processes. Lu et al. designed a PID controller based on self-adaptive state-space predictive functional control to enhance the ability in rejecting model mismatches and disturbance [19]. In [20], a robust gain-scheduled PID controller design for a linear-parameter-varying (LPV) system with parametric uncertainty is discussed. An internal model control (IMC)-PID controller is designed for the pole-zero shifted process with the shifting constant in [21]. A new tuning rule of PID controller is designed for first-order plus dead-time (FOPDT) systems where the relationships between the integral time/the derivative time and the time constant of FOPDT systems are built [22]. The influence of the sampling time on the discrete PID controllers is analyzed in [23] and the discrete implementation of a continuous controller is also discussed. A method of tuning the parameters of the continuous controller is presented, which is optimal according to the integral of time-weighted absolute error criterion in [24]. Some optimization algorithms, such as genetic algorithm (GA) [25], extremum seeking (ES) [26], particle swarm optimization (PSO) [27], fruit fly optimization [28], and Kronecker summation [29] are also proposed to optimize parameters of the PI/PID controller and these algorithms can ensure the satisfactory control performance with some performance indexes. Note that these tuning methods of the PI/PID controller have some limitations, some of them needs trials and errors, and some of them optimize parameters based on some performance indexes. In addition, a theory on the PID controller is proofed about the global stability and asymptotic regulation of the closed-loop control systems in [5] and a robust PID design based on quantitative feedback theory and convex-concave optimization is discussed in [30]. The theoretical studies such as the stabilizing PID controllers for time delay systems [31] and the PID design for the nonlinear system [32] are also reported recently.

The PID controller plays a non-substitutable role in process control, for example, the feedback controller in the coordinated control system (CCS), the most critical loop of a power plant is the PID controller to enhance the tracking speed and disturbance rejection ability [33]. Even though the PID controller roles as an important part in feedback control loops, how to design the suitable values of PI/PID parameters with a systematic procedure still is an open question. The relative delay margin (R_{dm}) has been proposed to optimize disturbance rejection performance of the PI controller [34]. However, how to design the PID controller with the relative delay margin has not been reported, to the authors' knowledge. To design the optimized PID controller with better disturbance rejection performance and desired robustness, the relative delay margin is proposed for the PID controller design. To obtain the explicit expressions of the proportional gain (k_p) and the integral gain (k_i), and the theoretical ranges of these two parameters, the relationship between the parameters of the proportional-integral-derivative controller and the new pair, e.g., the phase margin and the corresponding gain crossover frequency, is derived. Besides, the stability regions of the proportional gain (k_p) and the integral gain (k_i) are also

analyzed with constraints on the relative delay margin. Then an optimal disturbance rejection problem which is the tuning processes of the PID parameters is formulated and solved. Based on the above work, the tuning method for the PID controller is proposed to obtain satisfactory control performance with the desired robustness constraint.

The following interesting outcomes, as the main contributions of the paper, are derived in an innovative way:

(1) The PID tuning formula is analytically derived in terms of the relative delay margin for FOPDT systems.
(2) The stability regions for k_p and k_i based on a given derivative gain (k_d) and the process model are analyzed.
(3) The desired delay robustness-constrained optimization (DRO) for the PID controller is formulated and a set of recommended parameters is offered for the ease of use.
(4) Illustrative examples are carried out and results verify the superiority of the proposed DRO design for the PID controller.

The rest of this paper is organized as follows: the problem is formulated in Section 2. The basic control structure, and the research purpose to minimize the integral of the error with the fixed k_d and the delay margin constraint are introduced in this section. In Section 3, the PID tuning formula is derived in terms of the numerator and denominator of relative delay margin. Besides, a theorem about the ranges of k_p and k_i is given and the proof is also offered. Then the tuning method based on DRO is developed and solved analytically for the PID controller in Section 4. A set of recommended parameters is also offered for tuning parameters easily and conveniently in Section 4. In Section 5, simulations illustrate the superiority of the DRO tuning for the PID controller and the implementation of the derivative for practical applications is also discussed. Finally, Section 6 offers concluding remarks.

2. Problem Formulation

2.1. The Basic Control Structure

To better design the PID controller for a FOPDT model, the basic control structure is depicted as shown in Figure 1, where $G_p(s)$, $G_c(s)$, $F(s)$, and $H(s)$ are the FOPDT model, the PID controller, a set-point prefilter, and a feedback controller on the feedback path, respectively. The control structure is a typical two degrees of freedom (2-DOF) PID control system [8].
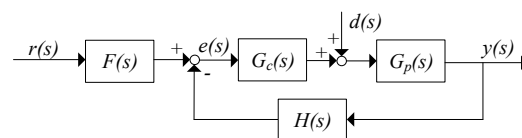

Figure 1. The structure of a two degrees of freedom proportional-integral-derivative (PID) system.

The process model is expressed as,

$$G_p(s) = \frac{K}{Ts+1}e^{-Ls},$$

(1)

where K, T, and L are the process gain, the time constant, and the delay time, respectively. Note that K, T, and L all have positive values for a stable process. The reason to study the FOPDT model is that the FOPDT model can reflect most dynamics of the real process and it can be used to approximate most of the industrial process [35]. Therefore, the proposed design method is deduced based on the FOPDT model in this paper. Note that it is not suitable for typical second order models which is discussed in Appendix A.

The output of the 2-DOF PID controller is expressed as,

$$u(t) = k_p \left[(br - y) + \frac{1}{T_i} \int_0^t (r - y)dt + T_d \frac{d(cr - y)}{dt} \right], \tag{2}$$

where k_p, T_i, and T_d are the proportional gain, the integral time, and the derivative time, respectively. Besides, r, y, and d are the reference, process output and input disturbance, respectively. When the set-point weighting factors (b and c) and $H(s)$ are set as 1, the typical 2-DOF PID controller becomes the conventional 1-DOF PID controller. By applying Laplace transform, the control law in Equation (2) has a set-point prefilter depicted by

$$F(s) = \frac{cT_iT_ds^2 + bT_is + 1}{T_iT_ds^2 + T_is + 1}, \tag{3}$$

and a feedback controller depicted by

$$G_c(s) = k_p \left(1 + \frac{1}{T_is} + T_ds \right). \tag{4}$$

The output y is decided by $Y(s) = G_{ry}(s)R(s) + G_{dy}(s)D(s)$, where $Y(s)$, $R(s)$, $D(s)$, $G_{ry}(s)$ and $G_{dy}(s)$ are the Laplace transforms of the output, the reference, the input disturbance, the transfer function from r to y and the transfer function from d to y, respectively. Besides, $G_{ry}(s)$ and $G_{dy}(s)$ are depicted by

$$G_{ry}(s) = \frac{F(s)G_c(s)G_p(s)}{1 + G_c(s)H(s)G_p(s)}, \tag{5}$$

and

$$G_{dy}(s) = \frac{G_p(s)}{1 + G_c(s)H(s)G_p(s)}. \tag{6}$$

We can know that the prefilter $F(s)$, or the set-point weighting factors (b and c) only influence the tracking performance. The disturbance rejection performance is only influenced by the feedback controller $G_c(s)$ without considering the mutual effects coming from residues. We have a view that the feedback controller $G_c(s)$ is tuned mainly for a desired disturbance rejection. The set-point weighting factors (b and c) are adjusted to obtain a desired tracking performance and further adjusted to enhance the disturbance rejection performance slightly [36]. Note that $H(s)$, the feedback controller on the feedback path, is set to one in this paper.

2.2. Problem Formulation

The purpose of the PID tuning is to obtain the minimum performance criterion, such as the integral squared error (ISE), the integrated absolute error (IAE) and the integral of time-weighted absolute error (ITAE) criteria, with the certain robustness constraint. This can be addressed in the following form:

$$\begin{cases} \text{Min performance criterion (ISE/IAE/ITAE),} \\ \text{Subject to robustness constraint } (M_s). \end{cases}$$

Even though ISE, IAE, and ITAE can be used as the performance criterions, the performance criterion, the integral of the error (IE), is recommended [11,34]. It is further revealed that,

$$\text{IE} = \int_0^\infty [r(t) - y(t)]dt = \frac{T_i}{k_p} = \frac{1}{k_i}, \tag{7}$$

which is for a stable closed-loop system with zero initial error and a unit step input disturbance [37]. Note that the IE criterion is chosen as the performance criterion considering that the smaller IE can

result in a larger k_i and IE has a quantitative relationship with k_i. In addition, a larger k_i can result in a stronger disturbance rejection ability. This idea of minimizing the value of IE is similar with that in [11] where the non-convex optimization problem is solved by the graphical method. Besides, IE can be seen as an approximation of IAE if the system has a slight oscillation. Note that the value of IE can be far from that of IAE for some special processes if the system has a serious oscillation or an inverse response, for example, for a process with one right half plane zero.

The maximum sensitivity function is often selected as the robustness index, and it is defined as,

$$M_s = \max_\omega \left| S(i\omega) \right| = \max_\omega \left| \frac{1}{1 + G_c(i\omega)G_p(i\omega)} \right|. \tag{8}$$

Its physical meaning is the reciprocal of the shortest distance from the critical point to the Nyquist curve and the reasonable range of M_s is 1.2~2.0. Some attempt for the tuning purpose is made by fitting it as a high-order polynomial in terms of parameters [38] or reducing it to a contour of numerous ellipses in the complex plane [11]. For controller synthesis, M_s constraint is often used to verify the robustness of the closed-loop system with designed parameters and cannot be used to optimize PID controller parameters systematically and directly [30,39]. Note that the optimization of M_s-constrained for the PID controller is feasible and reasonable for modern computers. To design the PID controller simply and directly, a new index called the delay margin, is chosen to represent the robustness index [40], which represents the maximum allowable delay variation and can be used to tune parameters directly. It is defined as,

$$R_{dm} = \frac{\varphi_m}{\omega_{gc}L}, \tag{9}$$

where φ_m, ω_{gc}, and L are the phase margin, the corresponding gain crossover frequency, and the delay time of the FOPDT model, respectively. The motivations to choose R_{dm} as the desired robustness measure are summarized as follows [34]:

(1) The maximum sensitivity function, M_s, is defined in the closed-loop form and this results in some difficulties in analysis. Besides, M_s is the maximum value of the sensitivity function over the whole frequency range. On the contrary, the delay margin is an open-loop measure with the information in a single point.
(2) As is well known, there is a fundamental limit on ω_{gc} for the processes with time delay, i.e., $\omega_{gc}L < 1$ [8]. Note that the qualitative inequality is extended for a quantitative purpose.
(3) The delay margin is dimensionless and can reflect the influence of the time delay on the variation in the delay time. Besides, the delay margin can be used to optimize parameters of the PID controller directly and easily as shown in next section. However, M_s is often used to test the robustness of the closed-loop system with designed parameters.

Note that the delay margin R_{dm} as a single measure of the desired robustness may have some limitations. The delay margin R_{dm} may not always ensure the good robustness of the closed-loop system when it is applied to test the robustness of the closed-loop system. Fortunately, the delay margin as an open-loop measure can be used to design the PID controller directly, and the PID controller based on the delay margin can ensure the desired robustness with a reasonable R_{dm} and a reasonable design procedure.

Above all, the problem formulation can be reorganized as:

$$\left\{ \begin{array}{l} \text{Min IE criterion with the fixed } k_d, \\ \text{Subject to the delay margin.} \end{array} \right. .$$

This means that the purpose of this research is to find the optimized parameters of the PID controller with the delay margin to enhance the disturbance rejection ability of the closed-loop system by a reasonable design procedure. In this research, the delay margin, as a desired robustness constant,

is proposed to design the optimized PID controller with the larger k_i. Besides, the stability regions of k_p and k_i with the delay margin are another concern considering that stability regions are necessary parts for a new design method.

Based on the problem formulation, the stability regions and the PID tuning with constraints on relative delay margin will be analyzed in the following section.

3. Stability Regions Based on the Relative Delay Margin

The tuning formula of the PID controller with the relative delay margin R_{dm} is deduced in this section. Then stability regions of PID parameters are obtained in terms of the new pair (φ_m and $\omega_{gc}L$). Note that the following deductions based on the regular variables are carried out. To simplify the analysis, the deductions with time scaling and dimensionless variables, as used in [41], are also given in Appendix B.

Based on the transfer function of the process model in Equation (1) and the feedback controller in Equation (4), the loop transfer function becomes,

$$G_l(i\omega) = \left(k_p + \frac{k_i}{i\omega} + k_d i\omega\right)\left(\frac{K}{1 + iT\omega}e^{-i\omega L}\right). \tag{10}$$

Equation (10) can be expanded in a rectangular form,

$$G_l(i\omega) = X_R + iY_I, \tag{11}$$

where

$$X_R = Kk_p\frac{\cos(L\omega) - T\omega\sin(L\omega)}{T^2\omega^2 + 1} - K\left(k_i - k_d\omega^2\right)\frac{\sin(L\omega) + T\omega\cos(L\omega)}{\omega(T^2\omega^2 + 1)}, \tag{12}$$

and

$$Y_I = -Kk_p\frac{\sin(L\omega) + T\omega\cos(L\omega)}{T^2\omega^2 + 1} - K\left(k_i - k_d\omega^2\right)\frac{\cos(L\omega) - T\omega\sin(L\omega)}{\omega(T^2\omega^2 + 1)}. \tag{13}$$

Note that the real and imaginary parts are both linear combinations of k_p, k_i, and k_d. The Nyquist plot of the loop transfer function should pass through the selected point, which is denoted as,

$$x_o = -\cos(\varphi_m) - i\sin(\varphi_m), \tag{14}$$

and the corresponding gain crossover frequency is ω_{gc}.

By equaling Equation (11) and Equation (14), we can obtain,

$$\begin{cases} Kk_p\frac{L(L\cos(a) - Ta\sin(a))}{T^2a^2 + L^2} - K\left(k_iL^2 - k_da^2\right)\frac{L\sin(a) + Ta\cos(a)}{a(T^2a^2 + L^2)} = -\cos(\varphi_m) & (15.1) \\ -Kk_p\frac{L(L\sin(a) + Ta\cos(a))}{T^2a^2 + L^2} - K\left(k_iL^2 - k_da^2\right)\frac{L\cos(a) - Ta\sin(a)}{a(T^2a^2 + L^2)} = -\sin(\varphi_m) & (15.2) \end{cases}, \tag{15}$$

where a dimensionless parameter is used as $a = \omega L$ to simplify the formula derivation.

By a simple transformation (we can obtain functions by Equation (15.1) $\times$ $\cos(a)$−Equation (15.2) $\times$ $\sin(a)$ and Equation (15.1) $\times$ $\sin(a)$+Equation (15.2) $\times$ $\cos(a)$, and then solve the obtained linear functions), the controller parameters can be obtained as follows,

$$\begin{cases} k_pK = \frac{T}{L}a\sin(\varphi_m + a) - \cos(\varphi_m + a) \\ K\left(k_iL^2 - k_da^2\right) = aL\sin(\varphi_m + a) + Ta^2\cos(\varphi_m + a) \end{cases}. \tag{16}$$

When the value of k_d in Equation (16) is obtained by Z-N stability criteria as the recommendation in [42], the integral time of the PID controller is,

$$\frac{k_p}{k_i L} = \frac{T_i}{L} = \frac{Ta\sin(\varphi_m + a) - L\cos(\varphi_m + a)}{aL\sin(\varphi_m + a) + Ta^2\cos(\varphi_m + a) + k_d Ka^2}. \tag{17}$$

Obviously, Equations (16) and (17) offer an elegant and simple tuning formula, which will be applied to the PID tuning directly in next section.

From Equation (16), the expression of k_i can be obtained as follows,

$$k_i = \frac{aL\sin(\varphi_m + a) + Ta^2\cos(\varphi_m + a)}{KL^2} + \frac{k_d a^2}{L^2}, \tag{18}$$

where k_i is determined by three parts from Equation (18). k_i is mainly determined by $a^2\cos(\varphi_m + a)$ for lag-dominant processes (large T/L) and mainly determined by $aL\sin(\varphi_m + a)$ for delay-dominant processes (small T/L) with a given k_d.

In order to obtain the stability regions of PID parameters k_p and k_i with a given k_d, a brief but somewhat less rigorous method will be given to determine the upper boundary of stability region in the situation of $\varphi_m = 0$ based on the work in [34].

The following lemmas will be used for the analysis of the stability regions of k_p and k_i [34,43]:

Lemma 1. *The inequity $k_i > 0$ is a necessary condition of the stability of the closed-loop system.*

Lemma 2. *The available range of k_d is $\left[-\frac{T}{K}, \infty\right)$, otherwise the closed-loop system is unstable.*

Lemma 3. *The inequities $\varphi_m \geq 0$ and $a \geq 0$ are necessary conditions of the stability of the closed-loop system.*

Theorem 1. *The range of k_p for the given FOPDT plant in Equation (1) can be stabilized with a PID controller is given by*

$$-\frac{1}{K} < k_p < \frac{1}{K}\left[\frac{T}{L}a_1\sin(a_1) - \cos(a_1)\right], \tag{19}$$

where a_1 is the root of the following equation,

$$\tan(a_1) = -\frac{T}{T+L}a_1, \tag{20}$$

and a_1 is in the interval of $\left(\frac{\pi}{2}, \pi\right)$.

For a given k_p locating in the range of Equation (20) and a given k_d determined by Z-N method, the range of k_i guaranteeing the stability of the closed-loop system is given by

$$0 < k_i < \max\left\{\frac{\alpha}{KL}\left[\sin(\alpha) + \frac{T}{L}\alpha\cos(\alpha)\right] + \frac{k_d\alpha^2}{L^2}\right\}, \tag{21}$$

where the maximum value of α is the root of the following equation,

$$k_p K - \frac{T}{L}\alpha\sin(\alpha) + \cos(\alpha) = 0, \tag{22}$$

and α is in the interval of $(0, a_1)$.

Proof. The lower boundary of the stability region of k_i is 0, which can be obtained by $a = 0$ and also can be obtained from Lemma 1. Let $\varphi_m = 0$, and the upper boundary of controller parameters can be obtained by the following expression,

$$\begin{cases} k_p K = \frac{T}{L} a \sin(a) - \cos(a) \\ K(k_i L^2 - k_d a^2) = aL \sin(a) + Ta^2 \cos(a) \end{cases}.$$
(23)

Let $z = L\omega$, and we can obtain the derivative of k_p as follows,

$$\frac{dk_p}{dz} = \frac{1}{K}\left[\sin(z) + \frac{T \sin(z)}{L} + \frac{Tz \cos(z)}{L}\right].$$
(24)

Firstly, we can know that $\frac{dk_p}{dz} \geq 0$ when $z \in \left[0, \frac{\pi}{2}\right]$, because that we have $\sin(z) \geq 0$, $\cos(z) \geq 0$ and $z \geq 0$.

Secondly, we can obtain the following expression,

$$\frac{d^2 k_p}{dz^2} = \frac{1}{K}\left[\cos(z) + \frac{2T \cos(z)}{L} - \frac{Tz \sin(z)}{L}\right],$$
(25)

where $z \in \left(\frac{\pi}{2}, a_1\right]$ and a_1 is the solution of the $\tan(a_1) = -\frac{T}{T+L}a_1$. As we know that $\cos(z) < 0$ and $z \sin(z) > 0$ when $\left(\frac{\pi}{2}, a_1\right]$ is the subaggregate of $\left(\frac{\pi}{2}, \pi\right)$, and $\frac{d^2 k_p}{dz^2} \leq 0$ is always tenable. This means that $\frac{dk_p}{dz}$ is a monotone decreasing function. What is more, $\left.\frac{dk_p}{dz}\right|_{z=a_1} = 0$ is tenable when a_1 is the solution of $\tan(a_1) = -\frac{T}{T+L}a_1$. Therefore, $\frac{dk_p}{dz} \geq 0$ is always tenable when $z \in [0, a_1]$. The lower and upper boundaries of k_p are obtained when $z = 0$ and $z = a_1$, respectively. Therefore, stability region of k_p can be obtained,

$$-\frac{1}{K} < k_p < \frac{1}{K}\left[\frac{T}{L}a_1 \sin(a_1) - \cos(a_1)\right].$$
(26)

For a given k_p in the range of Equation (26) and a given k_d in the stability region as depicted in Lemma 2, the corresponding α by solving,

$$k_p K - \frac{T}{L}\alpha \sin(\alpha) + \cos(\alpha) = 0.$$
(27)

However, the monotonicity of the expression of k_i, which is shown by

$$k_i = \frac{\alpha}{KL}\left[\sin(\alpha) + \frac{T}{L}\alpha \cos(\alpha)\right] + \frac{k_d \alpha^2}{L^2},$$
(28)

is changeable, and the upper boundary of k_i can be easily obtained by going through the achievable range of α, whose maximum value is determined by

$$k_p K - \frac{T}{L}\alpha \sin(\alpha) + \cos(\alpha) = 0,$$
(29)

and minimum value is determined by Lemma 1. Therefore, we have,

$$0 \leq k_i < \max\left\{\frac{\alpha}{KL}\left[\sin(\alpha) + \frac{T}{L}\alpha \cos(\alpha)\right] + \frac{k_d \alpha^2}{L^2}\right\},$$
(30)

where the maximum value of α is the root of Equation (27) and α is in the interval of $(0, a_1)$. □

Remark 1. *The analytical derivations for the stability regions of k_p and k_i do not need the input reference signal. The Theorem 1 and other conclusions are applicable to arbitrary input reference signals.*

Finally, an example of a lag-dominated process is used to show stability regions with different k_d, which is depicted as,

$$G_p(s) = \frac{1}{15s+1}e^{-s}. \tag{31}$$

The stability regions of k_p and k_i with different k_d are shown in Figure 2. In addition, the maximum value of k_i ($k_{i\max}$) and the corresponding α (α^*) with the different k_d are also shown in Figure 3.
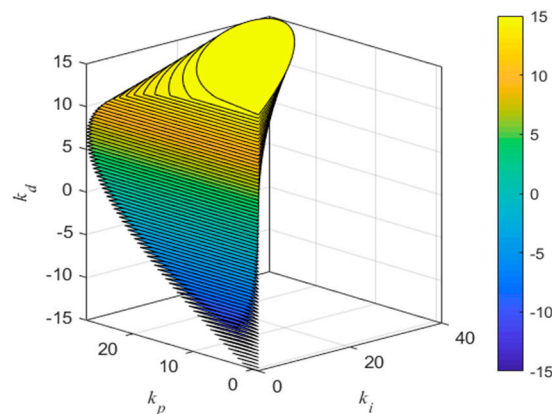

Figure 2. Stability region of k_p and k_i with different k_d.
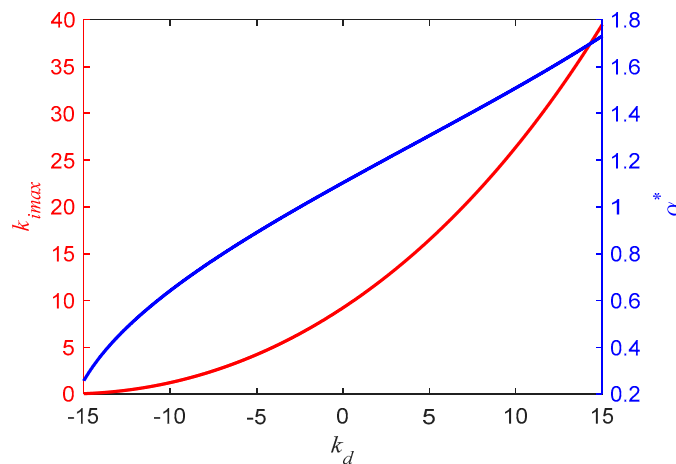
Figure 3. The value of $k_{i\max}$ and α^* with different k_d.

From Figures 2 and 3, we can know that the trends of k_p and k_i when k_d locates in the range of $\left[-\frac{T}{K}, \infty\right)$. Besides, the maximum value of k_i has a positive correlation relationship with that of k_d and α^* also has a similar relationship with k_d.

4. PID Tuning with Constraints on Relative Delay Margin

The loop transfer function with the process model in Equation (1) and the feedback controller in Equation (4) can be obtained,

$$G_L(\tilde{s}) = \left[\frac{T}{L}a\sin(\varphi_m+a) - \cos(\varphi_m+a) + \frac{a\sin(\varphi_m+a)+\frac{T}{L}a^2\cos(\varphi_m+a)}{\tilde{s}} + \frac{k_d a^2}{L\tilde{s}} + \frac{k_d K}{L}\tilde{s}\right]\frac{1}{1+\frac{T}{L}\tilde{s}}e^{-\tilde{s}}, \tag{32}$$

where $\tilde{s} = Ls$. The robustness indices, M_s and g_m, are determined by φ_m, a, and k_d when the process is given. The value of k_d can be obtained by Z–N method and can be adjusted based on the control

requirements. To better measure the lag/delay ratio for the process model, a normalized time delay is defined as [34],

$$\tau = \frac{L}{T + L},\tag{33}$$

where the range of τ is $[0, 1)$. A small τ means a lag-dominant process and a large τ means a delay-dominant process. The tuning of the PID controller with the purpose of obtaining the optimal disturbance rejection ability is analyzed as follows.

As the analysis in Section 2.2, the PID tuning with constraints on the relative delay margin can be formulated as,

$$\begin{cases} \max \ \frac{aL\sin(\varphi_m + a) + Ta^2\cos(\varphi_m + a)}{KL^2} + \frac{k_d a^2}{L^2}, \\ s.t. \ R_{dm} = \frac{\varphi_m}{a} = r_{dm} \text{ and a given } k_d, \end{cases}$$

where the objective function is a scaled integral gain in terms of φ_m, a, and k_d. r_{dm} is the representative of a desired robustness level and k_d is the desired value of the derivative gain. To solve the objective function, the derivative function with respect to a is obtained as follows,

$$\frac{d}{da}\left[\frac{aL\sin(a(r_{dm}+1)) + Ta^2\cos(a(r_{dm}+1))}{KL^2} + \frac{k_d a^2}{L^2}\right] = 0,\tag{34}$$

which can be further transformed to an algebraic equation,

$$\begin{aligned} \frac{1}{K}\big[\sin(a(r_{dm}+1)) + a\cos(a(r_{dm}+1))(r_{dm}+1) \\ + \frac{2Ta\cos(a(r_{dm}+1))}{L} - \frac{Ta^2\sin(a(r_{dm}+1))(r_{dm}+1)}{L}\big] + \frac{2k_d a}{L} = 0 \end{aligned}\tag{35}$$

where a is in the range of $(0, a_1)$, and Equation (35) can be solved numerically. Note that the deductions with time scaling and dimensionless variables about the PID tuning with constraints on relative delay margin are also offered in Appendix B for interested readers.

For a given process, PID controller parameters are determined by Equations (16) and (35) when k_d is determined by

$$k_d = k_g \frac{T}{K},\tag{36}$$

where k_g is the coefficient of T/K and the recommended range of k_g is $[0.1, 0.5]$. The reason choosing the given derivative gain in Equation (36) can been seen at the end of Section 3.1 in [42]: "The stabilizing sets of k_p and k_i in this case will also lie on the right side of the marginal stable boundary curve in (k_p, k_i) plane with increasing ω as det$\mathbf{J} = -K^2\omega$, which is $\forall \omega > 0$. There are various methods such as Ziegler–Nichols (Z–N) stability criteria, Integral of Square Error (ISE), Integral of Time Square Error (ITSE), Integral of Absolute Error (IAE), etc., by which one can choose the derivative gain k_d." Z–N stability criteria is chosen in this paper for convenience. Note that Equation (36) can avoid a large calculation load to obtain k_d even though it may not be the best choice. How to choose k_d more reasonably should be researched in the later work. The influence on a, k_i, and some conventional indices such as φ_m, g_m, and M_s with different k_g and r_{dm} can be seen in the Supplementary Materials.

Now, we can summarize the design procedure based on the discussion above as follows:

(1) The approximate FOPDT model (K, T, and L) is obtained by various approximation methods.
(2) The derivative gain k_d can be given by Equation (36) and a desired robustness level r_{dm} is also given. a can be obtained by solving Equation (35).
(3) k_p and k_i are calculated by Equation (16). Adjust the prefilter parameters (b and c) manually to obtain the satisfactory tracking performance.

The design procedure described above is named as DRO. Based on numerous simulations, the recommended parameters in terms of τ are listed in Table 1. Note that the control goal of the recommended parameters is to achieve a strong disturbance rejection ability and good tracking

performance with good robustness. The parameters of the prefilter, b and c, need to be manually tuned to improve the tracking performance. k_g needs to be manually tuned to enhance the disturbance rejection ability. R_{dm} can be obtained by the definition in Equation (9) with different ranges of τ. We can obtain that R_{dm} is equal to 1.8868, 1.9091, 1.9825, and 1.8852 for $\tau \leq 0.05$, $0.05 \leq \tau < 0.1$, $0.1 \leq \tau < 0.3$, and $\tau \geq 0.3$, respectively. Note that the recommended values of R_{dm} all locate in the range of $[1.7,\ 2.1]$ which is the reasonable range based on many simulation results. Besides, the parameters of DRO-PID (the PID controller designed by DRO) in Section 5 are all obtained based on the recommended parameters in Table 1.

Table 1. The recommended parameters of PID controller for delay robustness-constrained optimization (DRO) tuning.

Parameters	$\tau \leq 0.05$	$0.05 \leq \tau < 0.1$	$0.1 \leq \tau < 0.3$	$\tau \geq 0.3$
φ_m	1.00	1.05	1.13	1.15
a	0.53	0.55	0.57	0.61
b	0.6	0.6	0.6	0.6
c	1	1	1	1
k_g	0.3	0.2	0.2	0.2

Remark 2. *Parameters of the PID controller which need to be tuned are k_g, b, and c based on the tuning procedure with a desired R_{dm} or the pair of $\{\varphi_m,\ a\}$. k_p and k_i can be calculated by Equation (16) and are not adjusted manually. Different k_g, b, or c can result in different performance levels and how to adjust them may need the practice experience. To reduce the time spent and improve the control performance, the recommended parameters in Table 1 are suggested to calculate PID parameters quickly for interested readers. In fact, parameters of the proposed DRO-PID in the following illustrative examples are all obtained based on the recommended parameters in Table 1. Besides, how to choose b and c is discussed in Appendix C.*

5. Illustrative Examples

In this section, three illustrative examples are carried out to verify the efficacy of the proposed DRO-PID design, which is compared to other classic PID tuning methods [6,36] and DRO for the PI controller [34]. The IAE and the total variation of the control signal (TV) are used to measure the control performance. Their definitions are depicted as follows,

$$\text{IAE} = \int_0^\infty |r(t) - y(t)| dt, \tag{37}$$

and

$$\text{TV} = \sum_{i=1}^{n-1} |u(i+1) - u(i)|. \tag{38}$$

Note that indices of the tracking performance are the settling time (T_s), IAE_{sp}, and TV_{sp}. Indices of the disturbance rejection are IAE_{ud} and TV_{ud}. M_s is also used to measure the robustness of the closed-loop system. Besides, all following simulations use the "fixed-step" solver with the sampling time equating to 0.01 s.

5.1. Example 1

Consider a fourth-order process whose transfer function depicted as,

$$G_p(s) = \frac{1}{(s+1)^4}. \tag{39}$$

The approximate FOPDT is obtained for the DRO tuning,

$$\tilde{G}_p(s) = \frac{1}{2.1s + 1}e^{-1.9s}, \tag{40}$$

where the value of τ is 0.475. Based on Table 1, the value of R_{dm} is set as 1.8852 for the process in Equation (39) considering that the approximate FOPDT has $\tau \geq 0.3$. Note that the approximate FOPDT in Equation (40) is obtained based on the ***getfopdt*** function in [44].

Parameters of DRO-PID are obtained based on the model in Equation (40). Parameters of comparative controllers, such as the PI controller tuned by DRO (DRO-PI) [34], the PID controller tuned by SIMC (SIMC-PID) [6], and the PID controller tuned in [37] (Panagopoulos-PID) are also listed in Table 2. Note that parameters of DRO-PI, SIMC-PID, and Panagopoulos-PID are not tuned by the authors of this paper but are tuned by the authors in [6,34,37], respectively.

Table 2. Parameters of different controllers for Example 1.

Controllers	Parameters of Different Controllers
DRO-PID	$b = 0.6$, $c = 1$ *, $k_p = 0.8503$, $k_i = 0.3179$, $k_d = 0.4200$.
DRO-PI	$b = 0.6$ *, $k_p = 0.54$, $k_i = 0.2596$. [34]
SIMC-PID	$b = 1$, $c = 1$ *, $k_p = 0.5$, $k_i = 0.3333$, $k_d = 0.5$. [6]
Panagopoulos-PID	$T_f = 0.27$ *, $k_p = 1.14$, $k_i = 0.5112$, $k_d = 1.14$. [37]

* The prefilters are $F(s) = \frac{bT_i s + 1}{T_i s + 1}$ and $F(s) = \frac{1}{T_f s + 1}$ for DRO-PI and Panagopoulos-PID, respectively. SIMC-PID has the same prefilter with DRO-PID as depicted in Equation (3).

Output responses and the corresponding control signals are shown in Figures 4 and 5 respectively. Note that the step set-point and input disturbance are added to the system at 5 and 40 s, respectively. T_s, IAE_{sp}, and TV_{sp} are recorded from 5 to 40 s. IAE_{ud} and TV_{ud} are recorded from 40 to 80 s as listed in Table 3. M_s is also recorded in Table 3. Besides, the Nyquist diagram of the open-loop system with different controllers is also shown in Figure 6 where the unit circle centered at the origin and the circle centered at the $(-1, 0)$ with the radius $1/M_s$ are also given.
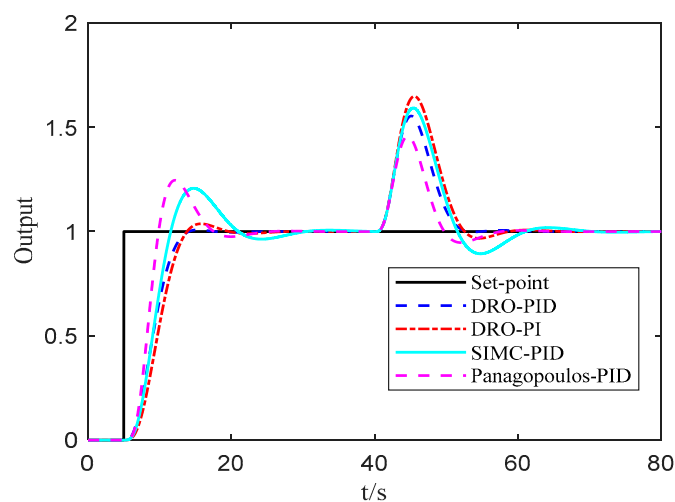

**Figure 4.** The output response of the step set-point and input disturbance for Example 1.
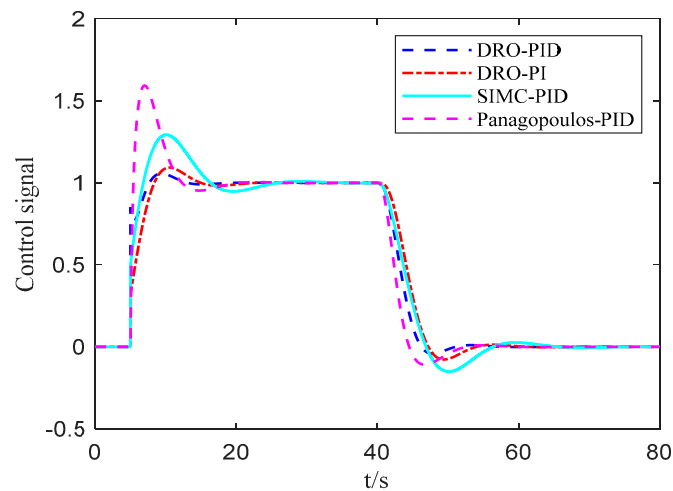
Figure 5. The control signal of the step set-point and input disturbance for Example 1.

Table 3. The indices of Example 1 with different controllers.

Controllers	T_s/s	IAE_{sp}	TV_{sp}	IAE_{ud}	TV_{ud}	M_s
DRO-PID	8.24	4.26	1.29	3.15	1.11	1.45
DRO-PI	12.83	4.96	1.23	4.10	1.18	1.58
SIMC-PID	22.38	5.39	1.71	4.22	1.36	1.48
Panagopoulos-PID	16.38	4.36	2.29	2.43	1.24	1.40
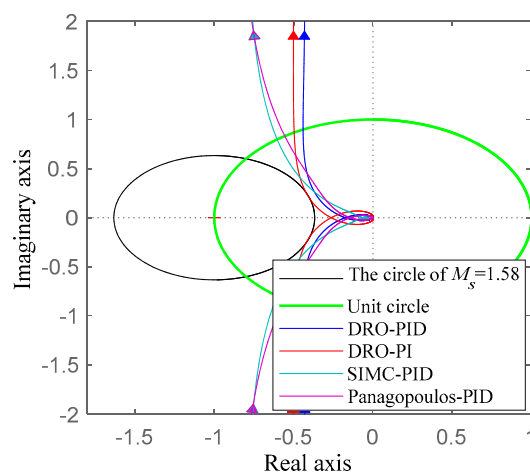
Figure 6. The Nyquist diagram for Example 1 with different controllers.

From Figure 4, DRO-PID has the smallest overshoot even though it has a slower response speed than SIMC-PID and Panagopoulos-PID. Besides, DRO-PID has the smallest T_s as listed in Table 3. IAE_{sp} also verifies that DRO-PID has the best tracking performance, which is about 80% of that of SIMC-PID. Panagopoulos-PID has serious oscillations even though it has the smallest IAE_{ud}. The disturbance output of DRO-PID has no oscillation. DRO-PID still has good robustness and M_s locates in the expected range of 1.2~2.0. From Figure 6, it can be seen that DRO-PID has better robustness than DRO-PI and SIMC-PID in the view of M_s even though the phase margin of DRO-PID is the smallest ($\varphi_m = 63.9°$). The TV of DRO-PID is smaller than that of SIMC-PID and Panagopoulos-PID as shown in Figure 5 and Table 3, which means DRO-PID can reduce the wear of actuators and is benefitting from the long running time. Therefore, DRO-PID has an advantage in obtaining approving tracking and disturbance rejection performance with the reasonable robustness constraint.

Finally, the ramp reference signal is added to the closed system to test the control performance for different input signals. The results are shown in Figures 7 and 8. The indexes are recorded in Table 4 (IAE_{sp} and TV_{sp} are recorded for the whole simulation). Note that the ramp set-point with a rate ±1/10 changes at 5 and 50 s, respectively. SIMC-PID and Panagopoulos-PID have larger overshoots (11.6% and 10.1%) than that of DRO-PID and DRO-PI (0.03% and 1.0%) even though they have a faster tracking speed. DRO-PID has the smallest T_s as listed in Table 4. Besides, IAE_{sp} of DRO-PID is smaller than that of DRO-PI and SIMC-PID, and is larger than that of Panagopoulos-PID. In general, DRO-PID can obtain satisfactory control performance with a small overshoot, IAE_{sp} and T_s for different input signals.
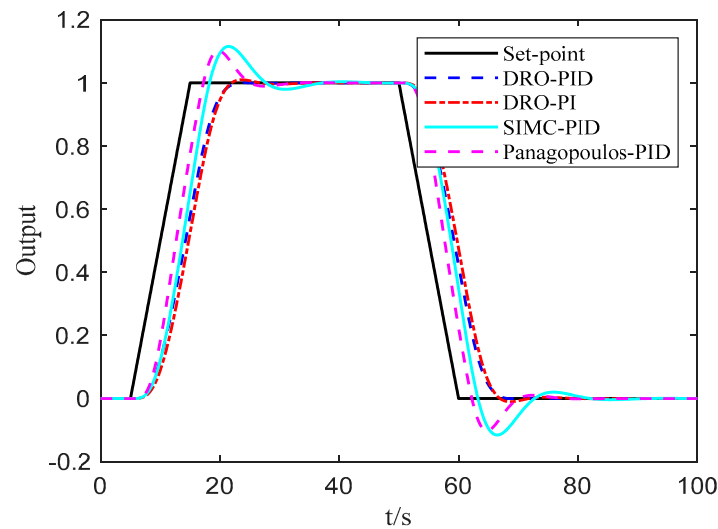
Figure 7. The output response of the ramp input for Example 1.
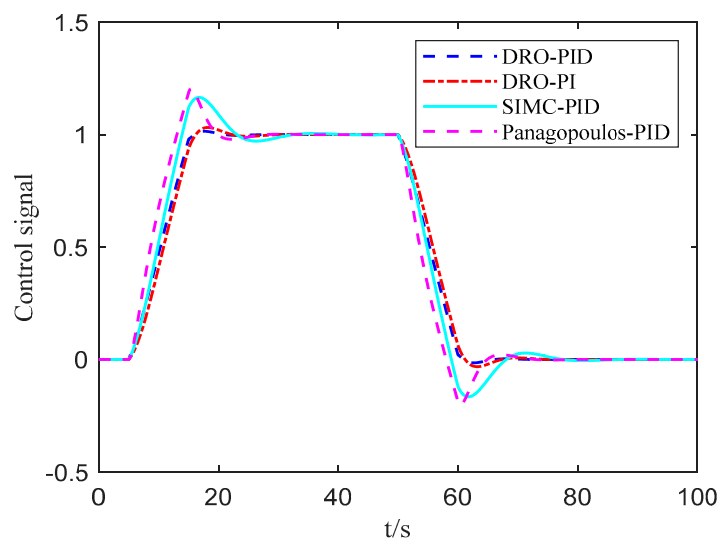
Figure 8. The control signal of the ramp input for Example 1.

Table 4. The indices of Example 1 with different controllers for the ramp input.

Controllers	T_s/s	IAE_{sp}	TV_{sp}
DRO-PID	15.95	8.43	2.07
DRO-PI	15.95	9.49	2.16
SIMC-PID	26.47	8.66	2.80
Panagopoulos-PID	18.75	6.27	2.90

5.2. Example 2

Consider a process which has one right half plane zero depicted as,

$$G_p(s) = \frac{1-2s}{(s+1)^3}. \tag{41}$$

The approximate FOPDT is obtained for DRO tuning,

$$\tilde{G}_p(s) = \frac{1}{1.822s+1}e^{-2.8s}, \tag{42}$$

where the value of τ is 0.606 and we have $R_{dm} = 1.8852$ for the process in Equation (41) considering that its approximate FOPDT has $\tau \geq 0.3$ based on Table 1. Note that the approximate FOPDT in Equation (42) is obtained based on the ***getfopdt*** function in [44]. Parameters of DRO-PID, DRO-PI, SIMC-PID, and Panagopoulos-PID are listed in Table 5. Note that parameters of DRO-PI, SIMC-PID, and Panagopoulos-PID are not tuned by the authors of this paper but are tuned by the authors in [6,34,37], respectively.

Table 5. Parameters of different controllers for Example 2.

Controllers	Parameters of Different Controllers
DRO-PID	$b = 0.6, c = 1$ *, $k_p = 0.5779, k_i = 0.2301, k_d = 0.3644$.
DRO-PI	$b = 1$ *, $k_p = 0.3376, k_i = 0.1858$. [34]
SIMC-PID	$b = 1, c = 1$ *, $k_p = 0.3, k_i = 0.2, k_d = 0.3$. [6]
Panagopoulos-PID	$b = 0.6$ *, $k_p = 0.542, k_i = 0.2618, k_d = 0.4282$. [37]

* The prefilter is $F(s) = \frac{bT_i s+1}{T_i s+1}$ for both DRO-PI and Panagopoulos-PID. SIMC-PID has the same prefilter with DRO-PID as depicted in Equation (3).

Output responses and the corresponding control signals of Example 2 are shown in Figures 9 and 10, respectively. Note that the step set-point and input disturbance are added to the system at 5 and 50 s, respectively. T_s, IAE$_{sp}$, TV$_{sp}$, IAE$_{ud}$, TV$_{ud}$, and M_s are all recorded in Table 6. Besides, the Nyquist diagram of the open-loop system with different controllers is shown in Figure 11 where the unit circle centered at the origin and the circle centered at the $(-1, 0)$ with the radius $1/M_s$ are also given.
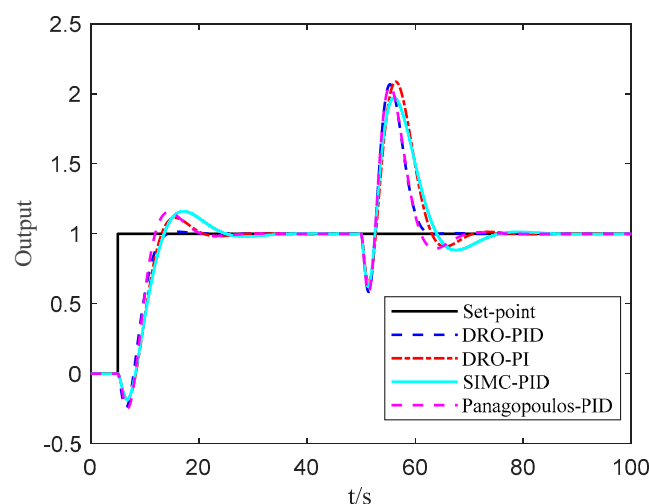

**Figure 9.** The output response of the step set-point and input disturbance for Example 2.
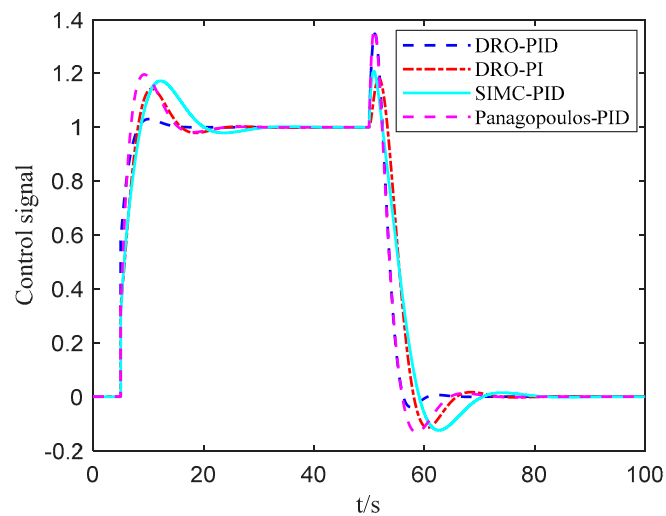
Figure 10. The control signal of the step set-point and input disturbance for Example 2.

Table 6. The indices of Example 2 with different controllers.

Controllers	T_s/s	IAE_{sp}	TV_{sp}	IAE_{ud}	TV_{ud}	M_s
DRO-PID	8.49	5.48	1.06	5.63	1.78	2.01
DRO-PI	14.81	6.44	1.33	7.36	1.63	2.02
SIMC-PID	18.76	7.14	1.39	7.71	1.70	1.73
Panagopoulos-PID	14.41	6.16	1.43	6.15	2.02	2.00
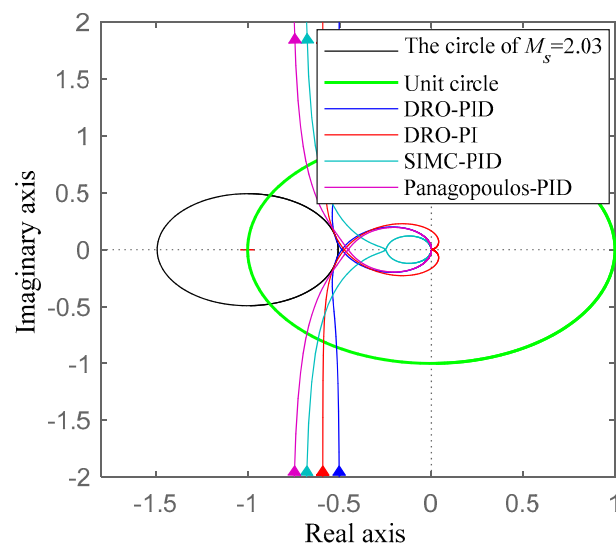
Figure 11. The Nyquist diagram for Example 2 with different controllers.

DRO-PID has the smallest overshoot (1.5%) while other three controllers have a large overshoot that are all larger than 14% as shown in Figure 9. DRO-PID has the smallest T_s as listed in Table 6. DRO-PID also has an obvious advantage in the disturbance rejection, and IAE_{ud} in Table 6 verifies this point. Besides, the TV_{sp} of DRO-PID is the smallest even though TV_{ud} of DRO-PID is larger than DRO-PI and SIMC-PID. Even though values of M_s for DRO-PID, DRO-PI, and Panagopoulos-PID are close to the upper boundary of the expected range, these controllers still can ensure a good robustness. DRO-PID has a similar gain margin with that of DRO-PI and Panagopoulos-PID, and SIMC-PID has a largest gain margin as shown in Figure 11. The phase margin of DRO-PID is the smallest ($\varphi_m = 58.9°$). Even though the robustness of DRO-PID has no advantage over the comparative controller, the control

performance of DRO-PID has obvious advantages over other controllers as shown in Figure 9 and Table 6.

Discussion: The IE indexes (for tracking performance) of DRO-PID, DRO-PI, SIMC-PID, and Panagopoulos-PID are 5.35, 5.38, 5.00, and 4.65, respectively, as shown in Figure 9. All of them have typical inverse responses caused by the right half plane zero. In fact, these four controllers are designed based on the approximate FOPDT in Equation (42) and DRO-PID obtains the minimum IE index based on the model in Equation (42) as shown in the Supplementary Materials. The Supplementary Materials contains the responses of the approximate FOPDT model in Equation (42) with the fixed parameters in Table 5. The relevant indexes are recorded and the Nyquist diagram of the open-loop system with different controllers are also given in the Supplementary Materials. We can know that DRO-PID has the best tracking and disturbance rejection performance with the smallest overshoot and settling time for the approximate FOPDT model in Equation (42). DRO-PID has good robustness and DRO-PID has a smaller M_s than that of DRO-PI and Panagopoulos-PID. Figures 9 and 10 are the responses with the process model in Equation (41) with these designed controllers.

This example can illustrate that DRO-PID designed based on the FOPDT model is also suitable for these processes with one right half plane zero even though the IE index of DRO-PID has no advantage which is caused by the inverse response of the non-minimum phase plant. The IE index is applied to optimize the parameters of DRO-PID by minimizing IE and obtaining the maximum k_i based on the approximate FOPDT model in this paper. The IAE index, the widely used measure, is applied to measure the performance of the closed-loop systems. Note that the design method for the non-minimum phase processes may be not be rigorous as discussed above where the IE indexes (for tracking performance) of DRO-PID is not the smallest. However, the successful application of the proposed DRO-PID designed for the non-minimum phase plant expands the controlled processes which can be approximated into FOPDT models.

5.3. Example 3

Consider an IPTD process whose transfer function depicted as,

$$G_p(s) = \frac{0.2}{s}e^{-7.4s}. \tag{43}$$

The approximate FOPDT is obtained for DRO tuning,

$$\tilde{G}_p(s) = \frac{200}{1000s+1}e^{-7.4s}, \tag{44}$$

where the value of τ is 0.0073 and we have $R_{dm} = 1.8868$ for the process in Equation (43) considering that its approximate FOPDT has $\tau \leq 0.05$. Note that the approximate method to obtain the FOPDT in Equation (44) is introduced in [8] and the FOPDT system is used to design the controller in [34]. The parameters of DRO-PID, DRO-PI, SIMC-PID, and Panagopoulos-PID are listed in Table 7. Note that the parameters of DRO-PI, SIMC-PID, and Panagopoulos-PID are not tuned by the authors of this paper but are tuned by the authors in [6,34,37], respectively.

Table 7. Parameters of different controllers for Example 3.

Controllers	Parameters of Different Controllers
DRO-PID	$b = 0.6$, $c = 1$ *, $k_p = 0.3716$, $k_i = 0.0079$, $k_d = 1.5$.
DRO-PI	$b = 0.6$ *, $k_p = 0.290$, $k_i = 0.0075$. [34]
SIMC-PID	$b = 1$, $c = 1$ *, $k_p = 0.3378$, $k_i = 0.0057$, $k_d = 1.5$. [6]
Panagopoulos-PID	$b = 1$ *, $k_p = 0.293$, $k_i = 0.0056$, $k_d = 1.409$. [37]

* The prefilter is $F(s) = \frac{bT_i s+1}{T_i s+1}$ for both DRO-PI and Panagopoulos-PID. SIMC-PID has the same prefilter with DRO-PID as depicted in Equation (3).

Output responses and the corresponding control signals of Example 3 are shown in Figures 12 and 13, respectively. Note that the step set-point and input disturbance are added to the system at 10 and 350 s, respectively. All indices are listed in Table 8 and the Nyquist diagram of the open-loop system with different controllers is also shown in Figure 14 where the unit circle centered at the origin and the circle centered at the $(-1, 0)$ with the radius $1/M_s$ are also given.

Again, we can know that DRO-PID has the smallest overshoot (3%) while other three controllers have a large overshoot ($\geq 9\%$) as shown in Figure 12. DRO-PID has a smaller T_s than that of SIMC-PID and Panagopoulos-PID even though the settling time of DRO-PID is larger than that of DRO-PI. IAE$_{sp}$ in Table 8 shows the advantage of DRO-PID in the tracking performance. Besides, DRO-PID has an obvious advantage in the disturbance rejection compared with other three controllers, and IAE$_{ud}$ in Table 8 also verifies this conclusion. However, the TV$_{sp}$ and TV$_{ud}$ of DRO-PID has no obvious advantage. All values of M_s locates in the expected range of 1.2~2.0 and can guarantee good robustness. DRO-PID has similar robustness with SIMC-PID. They have a smaller M_s than DRO-PI. From Figure 14, it can be seen that DRO-PID has a larger phase margin than SIMC-PID and Panagopoulos-PID. Therefore, DRO-PID has the best control performance with good robustness as shown in Figure 12 and Table 8.
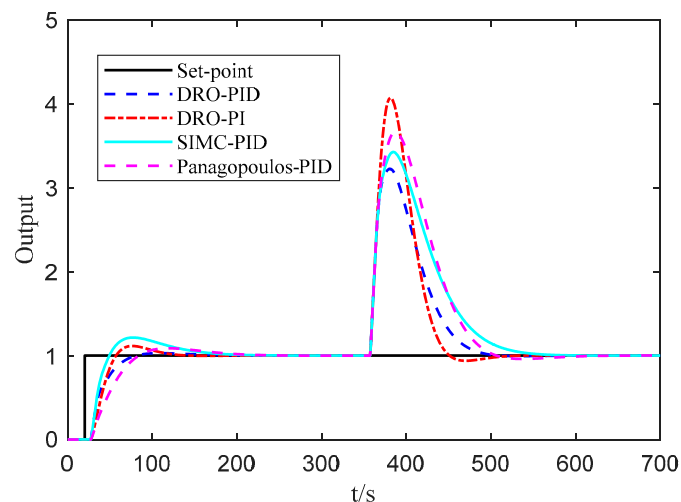

Figure 12. The output response of the step set-point and input disturbance for Example 3.
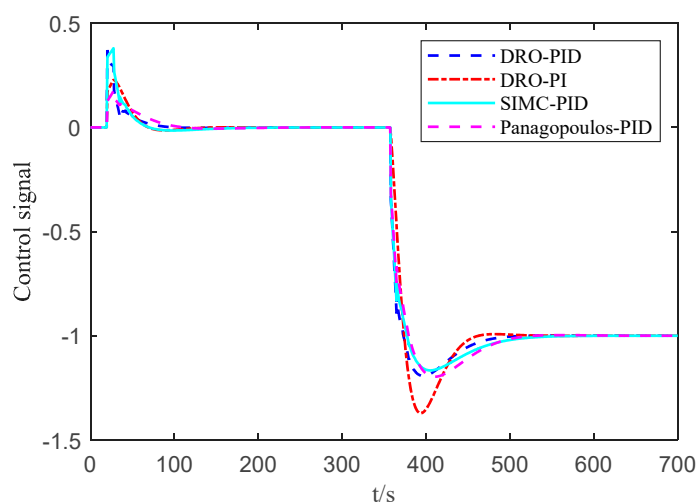

Figure 13. The control signal of the step set-point and input disturbance for Example 3.

Generally, the proposed DRO-PID can obtain the better tracking and disturbance rejection performance with the desired robustness contrasts based on the simulation results of Examples 1–3. The main reason is that the DRO-PID is designed by minimizing the IE index as discussed in Section 4. Therefore, the DRO-PID has a larger k_i which can ensure the closed-loop system has a stronger disturbance rejection ability. Then the tracking performance can be adjusted by the set-point prefilter. With the tuning procedure and the set of the recommended parameters, the DRO-PID can obtain the better control performance than other comparative PID controllers.

Table 8. The indices of Example 3 with different controllers.

| Controllers	T_s/s	IAE$_{sp}$	TV$_{sp}$	IAE$_{ud}$	TV$_{ud}$	M_s
DRO-PID	117.49	23.04	0.83	128.06	1.58	1.58
DRO-PI	100.31	25.04	0.49	138.65	1.76	1.68
SIMC-PID	160.29	31.29	0.85	175.27	1.52	1.54
Panagoulos-PID	175.71	35.88	0.38	184.39	1.57	1.47
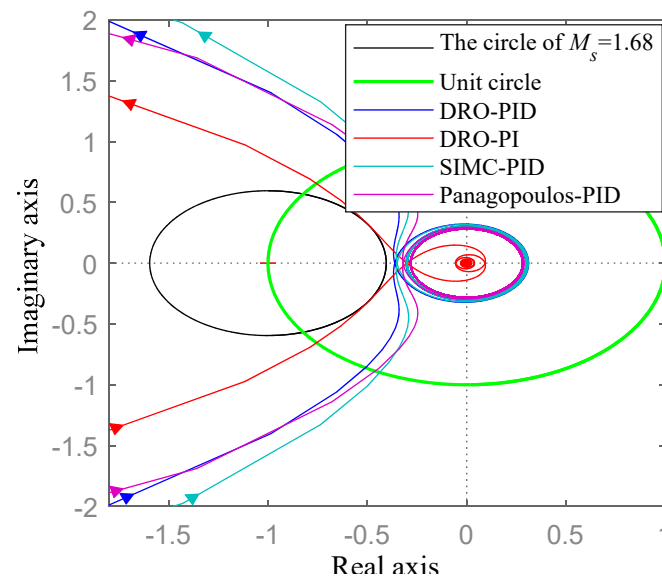
Figure 14. The Nyquist diagram for Example 3 with different controllers.

5.4. Discussion about the Implementation of the Derivative

Based on the simulation results of these three examples, the superiority of the proposed DRO-PID is verified. Note that the ideal derivative is applied in above theoretical analysis and simulations. However, the high-frequency measurement noise always exists in practical systems. The ideal derivative can amplify the high-frequency noise greatly which can generate large variations of the control signal. To weaken the adverse influence, a filtered derivative is used to replace the ideal derivative for the practical applications and the PID controller with the filtered derivative can be depicted by

$$G_c(s) = k_p\left(1 + \frac{1}{T_i s} + \frac{T_d s}{1 + T_d s/N}\right), \tag{45}$$

where N is the filter coefficient and the values of N are 2–20 [8]. With the filtered derivative, the variations of the control signal can be reduced reasonably. To explain this better, Example 1 depicted in Equation (39) is taken an example and the high-frequency measurement noise is added to the system output. The filter coefficient N is set as 20 and 2, and the parameters of DRO-PID are the same with that in Table 2. Besides, the step set-point and input disturbance are added to the system at 5 and 40 s, respectively. Note that the measurement noise is generated by MATLAB/SIMULINK "band-limited

white noise" with power = 0.00001, sample time = 0.01 s, and seed = [23341]. The results of the high-frequency attenuation ability can be seen in Figures 15 and 16.
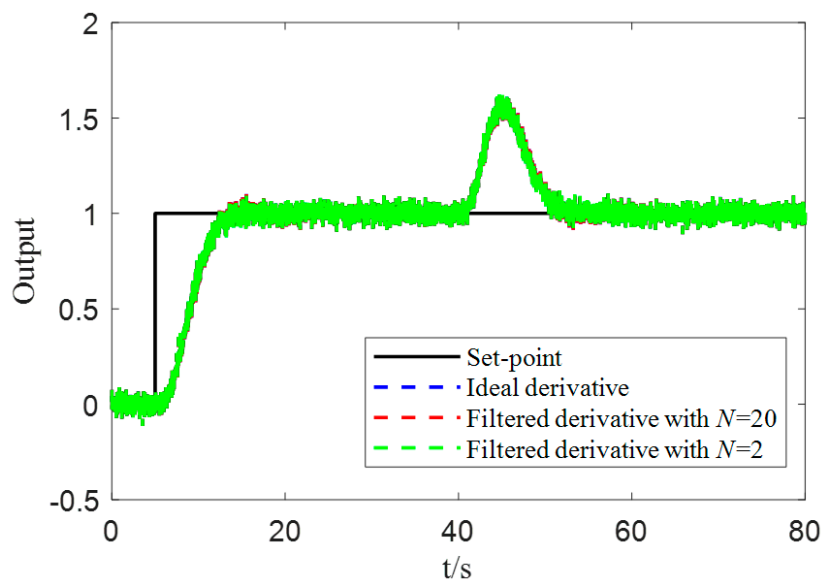

Figure 15. The output response for Example 1 with high-frequency measurement noise.
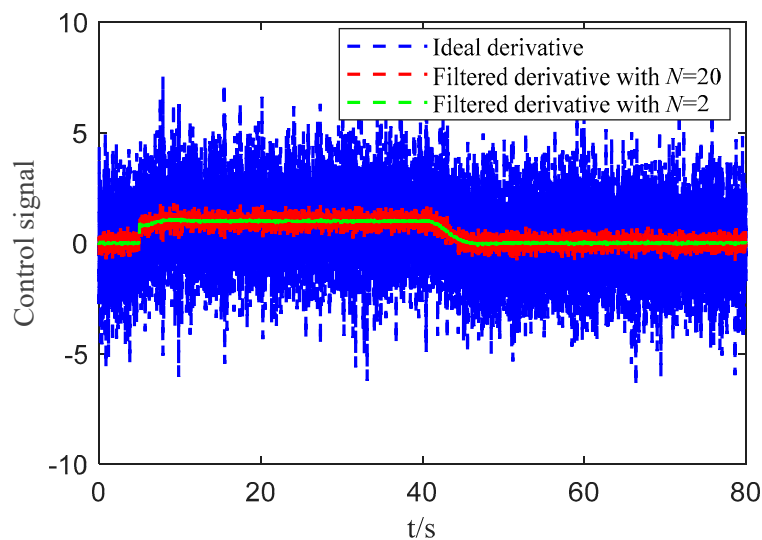

Figure 16. The control signal for Example 1 with high-frequency measurement noise.

It can be seen that the variations of the control signal was reduced greatly as shown in Figure 16 even though the filtered derivative has slight influence on the control performance. In addition, a smaller N can result in a smaller fluctuation range and a strong reduction capability of the measurement noise. However, the theoretical ranges of k_p and k_i with the filtered derivative in Theorem 1 may be different considering that the DRO-PID is proposed and analyzed for the ideal derivative. This should be discussed in future work. Even though DRO-PID is proposed and analyzed for the ideal derivative, the satisfactory control performance still can be obtained with the filtered derivative and other unchanged parameters. Therefore, the PID controller depicted in Equation (45) can also be designed by the proposed method and is recommended for practical applications to weaken the influence of the high-frequency measurement noise. What is more, how to choose a reasonable filter coefficient depends on the balance between the reduction capability of the measurement noise and the control

requirements. A smaller filter coefficient means a good reduction capability and the slight decrease in control performance, and vice versa.

5.5. Discussion about the Relationship between M_s and R_{dm}

Based on deductions in Sections 3 and 4 and simulations in Section 5, the relationship between M_s and R_{dm} are discussed in this subsection. As discussion in Section 2.2, M_s and R_{dm} are defined in the closed-loop form and open loop form, respectively. To obtain the maximum value of the sensitivity function, all frequency should be traversed over the whole frequency range, which relies on the numerical calculation. The calculation of R_{dm} relies on the phase margin, the corresponding gain, and the delay time of the FOPDT model. We cannot obtain the theoretical relation between M_s and R_{dm} directly and this can be studied in detail in future work. However, the relationship between M_s and R_{dm} can be presented based on illustrative examples by the numerical calculation.

Consider the lag-dominated process in Equation (31), the stable region of the PID controller (k_p and k_i with $k_d = 0.2\frac{T}{K} = 3.8$), the parameter pair $\{k_p, k_i\}$ with the same k_d and $R_{dm} = 1.40$, and the contour of $M_s = 1.64$ based on the method proposed in [11] are obtained as shown in Figure 17. It is surprising to find that the region of k_p and k_i decided by the delay margin $R_{dm} = 1.40$ has a similar region with that of $M_s = 1.64$. This means that M_s and R_{dm} can offer the similar parameter ranges. In other words, it implies that the R_{dm} can represent a reasonable robustness region even though the theoretical relation between M_s and R_{dm} cannot be given quantitatively.
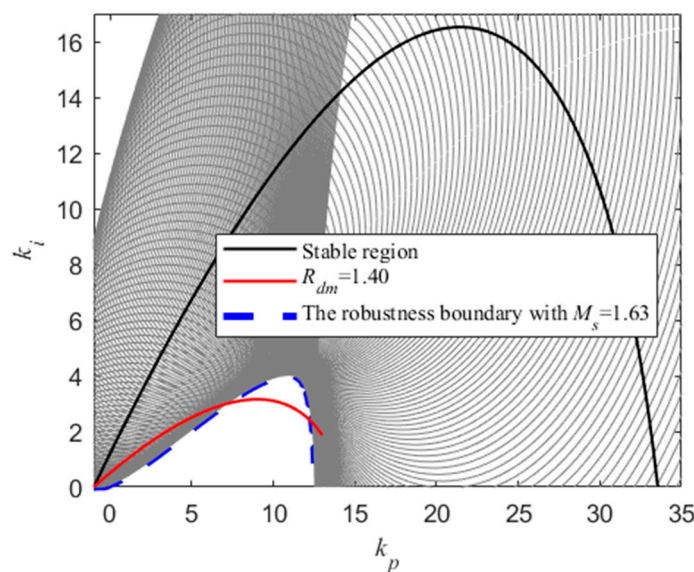

Figure 17. The distribution of k_p and k_i with $k_d = 3.8$.

Based on the tuning procedure in Section 4, the recommended ranges of k_g and R_{dm} are $[0.1, 0.5]$ and $[1.7, 2.1]$, respectively. Therefore, the simulation is carried out within these ranges. Figure 18 shows the distribution of M_s with different k_g and R_{dm} for Examples 1 and 3, respectively. Obviously, M_s of the closed-loop system locates in the reasonable range $[1.2, 2.0]$ when parameters of PID controller are tuned based on the proposed DRO tuning as discussed in Section 4. The simulation results verify the effectiveness of the delay margin when it is used to design the PID controller directly as a desired robustness measure.
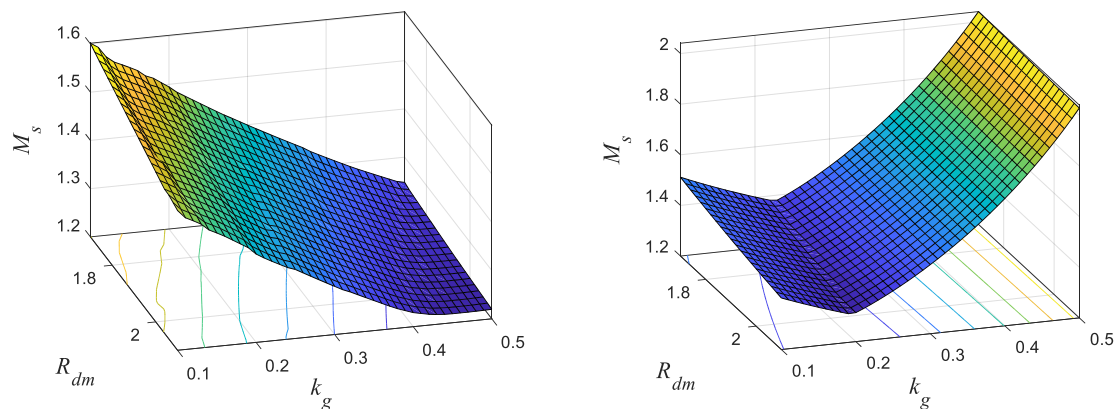
Figure 18. The distribution of M_s with different k_g and R_{dm} for Example 1 (**left**) and Example 3 (**right**).

Generally, the proposed DRO tuning can ensure satisfactory robustness. Note that the theoretical relation between the maximum sensitivity function M_s and the delay margin R_{dm} is not clear currently and should be studied in detail in the later work.

Besides, the controlled plants of three examples presented in Sections 5.1–5.3 are a fourth-order process, a process of one right half plane, and an IPTD process, respectively. The parameters of the proposed PID controller are obtained based on the tuning procedure in Section 4 and the approximate FOPDT models. The superiority of the proposed DRO tuning is verified to obtain satisfactory control performance with good robustness. Besides, the superiority of the proposed DRO tuning for FOPDT model is also verified as shown in the Supplementary Materials. These results illustrate that the proposed DRO tuning has an advantage over other comparative tuning rules for not only FOPDT processes but also other processes which can be approximated into FOPDT models.

6. Conclusions

This paper proposed the relative delay margin for the proportional-integral-derivative controller design. The relative delay margin can measure the desired robustness of the system and can be used to tune the proportional-integral-derivative parameters directly. Firstly, the proportional-integral-derivative tuning formula was analytically derived in terms of the numerator and denominator of relative delay margin. Based on the proportional-integral-derivative tuning formula, stability regions of the proportional-integral-derivative parameters k_p and k_i with a given k_d were determined in a simple way. A theorem about the ranges of k_p and k_i was given and the proof was also offered. Then the delay robustness-constrained optimization for the proportional-integral-derivative controller was formulated and the tuning method was also summarized as discussed in Section 4. A set of recommended parameters was also offered for tuning parameters easily and conveniently. The simulations were carried out for a fourth-order process, a process with one right half plane zero, and an integral process where the proposed proportional-integral-derivative controller are designed based on the recommended parameters. Besides, the comparative controllers (Skogestad internal model control, proportional-integral-derivative controller tuned by Panagopoulos, and PI controller tuned by delay robustness-constrained optimization) are designed by the authors in the relevant literature. Based on the simulation results, the proposed proportional-integral-derivative controller tuned by the delay robustness-constrained optimization can enhance the tracking performance and disturbance rejection performance simultaneously with the desired robustness constraints. For example, the integrated absolute errors of the proposed proportional-integral-derivative controller for the tracking performance and disturbance rejection performance are less than 91.3% and 91.7% of the integrated absolute errors of other comparative controllers in Example 3, respectively. This shows great potential in industrial applications. Besides, the proportional-integral-derivative controller with filtered derivative designed

by the proposed method is recommended for practical applications to weaken the adverse influence of the high-frequency measurement noise.

The main contributions of this paper can be summarized as:

(1) The PID tuning formula is analytically derived in terms of the relative delay margin for first order plus dead-time systems.

(2) A theorem about the ranges of k_p and k_i is given and the proof is also offered.

(3) The design method based on the delay robustness-constrained optimization for the proportional-integral-derivative controller is given and a set of recommended parameters is offered for the ease of use.

(4) Illustrative examples are carried out and results verify the superiority of the proposed proportional-integral-derivative controller design method.

The value of k_d decided by $k_d = k_g \frac{T}{K}$ may be a limitation of this paper and more optimized approaches of the choice of k_d should be studied in detail to improve the control performance in later work. Besides, the theoretical relation between M_s and R_{dm} also should be another interesting topic in future work.

Nomenclature

The symbols used in this paper are listed in this section.

g_m	The gain margin
M_s	The maximum sensitivity function
ω_{gc}	The gain crossover frequency
k_i	The integral gain of the PID controller
$G_p(s)$	The transfer function of the controlled plant
$F(s)$	The set-point prefilter
K	The process gain
L	The delay time
T_d	The derivative time of the PID controller
y	The process output
c	The set-point weighting factor
$Y(s)$	The Laplace transforms of the output
$D(s)$	The Laplace transforms of the input disturbance
$G_{dy}(s)$	The transfer function from the input disturbance to the output
$G_l(s)$	The open loop transfer function
s	The Laplacian operator
τ	The normalized time delay
TV	The total variation of control signal
$\tilde{G}_p(s)$	The approximate FOPDT model
φ_m	The phase margin
R_{dm}	The relative delay margin
k_p	The proportional gain of the PID controller

k_d The derivative gain of the PID controller
$G_c(s)$ The transfer function of the PID controller
$H(s)$ The feedback controller on the feedback path
T The time constant
T_i The integral time of the PID controller
r The reference signal
d The input disturbance
b The set-point weighting factor
$R(s)$ The Laplace transforms of the reference
$G_{ry}(s)$ The transfer function from the reference to the output
IE   The integral of the error
a The dimensionless parameter, $a = \omega L$
$\tilde{s}$ $\tilde{s} = Ls$
IAE   The integrated absolute error
T_s The settling time
N The filter coefficient and

Appendix A

In this section, the reason that the proposed design method is not suitable for typical second order models is discussed.

Consider a typical second order plant,

$$G_p(s) = \frac{K}{T_1 s^2 + T_2 s + 1} e^{-Ls}. \tag{A1}$$

The loop transfer function becomes Equation (A2) based on the plant in Equation (A1) and the PID controller,

$$G_l(i\omega) = \left(k_p + \frac{k_i}{i\omega} + k_d i\omega\right)\left(\frac{K}{1 + iT_2\omega - T_1\omega^2} e^{-i\omega L}\right). \tag{A2}$$

Equation (A2) can be expanded in a rectangular form,

$$G_l(i\omega) = X_R + iY_I, \tag{A3}$$

where

$$X_R = Kk_p \frac{\left(1 - T_1\omega^2\right)\cos(L\omega) - T_2\omega\sin(L\omega)}{T_2^2\omega^2 + \left(1 - T_1\omega^2\right)^2} - K\left(k_i - k_d\omega^2\right)\frac{\left(1 - T_1\omega^2\right)\sin(L\omega) + T_2\omega\cos(L\omega)}{\omega\left(T_2^2\omega^2 + \left(1 - T_1\omega^2\right)^2\right)}, \tag{A4}$$

and

$$Y_I = -Kk_p \frac{\left(1 - T_1\omega^2\right)\sin(L\omega) + T_2\omega\cos(L\omega)}{T_2^2\omega^2 + \left(1 - T_1\omega^2\right)^2} - K\left(k_i - k_d\omega^2\right)\frac{\left(1 - T_1\omega^2\right)\cos(L\omega) - T_2\omega\sin(L\omega)}{\omega\left(T_2^2\omega^2 + \left(1 - T_1\omega^2\right)^2\right)}. \tag{A5}$$

Note that the real and imaginary parts are both linear combinations of k_p, k_i and k_d. The Nyquist plot of the loop transfer function will pass through the selected point, which is denoted as,

$$x_o = -\cos(\varphi_m) - i\sin(\varphi_m), \tag{A6}$$

and the corresponding gain crossover frequency is ω_{gc}.

By equaling Equation (A3) and Equation (A6), we can obtain,

$$
\begin{cases}
Kk_pL^2\frac{(L^2-T_1a^2)\cos(a)-T_2aL\sin(a)}{T_2^2a^2L^2+(L^2-T_1a^2)^2} - L(k_iL^2-k_da^2)\frac{(L^2-T_1a^2)\sin(a)+T_2aL\cos(a)}{a(T_2^2a^2L^2+(L^2-T_1a^2)^2)} = -\cos(\varphi_m) & \text{(A7.1)} \\
-Kk_pL^2\frac{L((L^2-T_1a^2)\sin(a)+T_2aL\cos(a))}{T_2^2a^2L^2+(L^2-T_1a^2)^2} - KL(k_iL^2-k_da^2)\frac{(L^2-T_1a^2)\cos(a)-T_2aL\sin(a)}{a(T_2^2a^2L^2+(L^2-T_1a^2)^2)} = -\sin(\varphi_m) & \text{(A7.2)}
\end{cases}
\quad , \quad \text{(A7)}
$$

where a dimensionless parameter is used as $a = \omega L$ to simplify the formula derivation.

By a simple transformation (we can obtain functions by Equation (A7.1) $\times$ $\cos(a)-$Equation (A7.2) $\times$ $\sin(a)$ and Equation (A7.1) $\times$ $\sin(a)+$Equation (A7.2) $\times$ $\cos(a)$, and then solve the obtained linear functions), the controller parameters can be obtained as follows,

$$
\begin{cases}
k_pK = \frac{T_2}{L}a\sin(\varphi_m+a) - \left(1-\frac{T_1a^2}{L^2}\right)\cos(\varphi_m+a) \\
K(k_iL^2-k_da^2) = aL\left(1-\frac{T_1a^2}{L^2}\right)\sin(\varphi_m+a) + Ta^2\cos(\varphi_m+a)
\end{cases}
\quad . \quad \text{(A8)}
$$

From Equation (A8), the expression of k_i can be obtained as follows,

$$
k_i = \frac{aL\left(1-\frac{T_1a^2}{L^2}\right)\sin(\varphi_m+a) + Ta^2\cos(\varphi_m+a)}{KL^2} + \frac{k_da^2}{L^2}. \tag{A9}
$$

We can obtain the derivative of k_p in respect to a as follows,

$$
\frac{dk_p}{da} = \frac{1}{KL^2}\left[(T_2L+2T_1)a\cos(a) + \left(T_2L+L^2-T_1a^2\right)\sin(a)\right]. \tag{A10}
$$

Then we can obtain the following expression

$$
\frac{d^2k_p}{da^2} = \frac{1}{KL^2}\left[\left(2T_2L+2T_1+L^2-T_1a^2\right)\cos(z) - a(T_2L+4T_1)\sin(a)\right]. \tag{A11}
$$

Based on the Equations (A10) and (A11), we can know that the sign of $\frac{dk_p}{da}$ depends on the value of T_2, T_1, and L, which means that the different second order plants may have different results about the sign of $\frac{dk_p}{da}$. Therefore, the upper limit of k_i cannot be obtain based on the analytical derivations.

Appendix B

In this part, the deductions about the stability regions with time scaling and dimensionless variables, as used in [41], are given.

Based on the process model in Equation (1) and the PID controller in Equation (4), the process model with time scaling and the PID controller with dimensionless variables can be depicted as,

$$
G_{po}(s_o) = \frac{1}{s_o+1}e^{-\theta s_o}, \tag{A12}
$$

and

$$
G_{co}(s_o) = k_{po}\left(1+\frac{1}{T_{io}s_o}+T_{do}s_o\right) = k_{po}+\frac{k_{io}}{s_o}+k_{do}s_o, \tag{A13}
$$

where the operator "s" is replaced by $s_o = Ts$. Correspondingly, we have $\theta = L/T$, $k_{po} = Kk_p$, $T_{io} = T_i/T$, $T_{do} = T_d/T$, $k_{io} = KTk_i$, $k_{do} = k_dK/T$, and $\omega_o = \omega T$ [41]. Note that the definition of the delay margin in Equation (9) becomes,

$$
R_{dm} = \frac{\varphi_m}{\omega_{gco}\theta}, \tag{A14}
$$

which is equivalent to Equation (9). The loop transfer function with a rectangular form can be depicted as,

$$G_{lo}(i\omega_o) = X_R + iY_I,$$ (A15)

where

$$X_R = k_{po}\frac{\cos(\theta\omega_o) - \omega\sin(\theta\omega_o)}{\omega_o^2 + 1} - \left(k_{io} - k_{do}\omega_o^2\right)\frac{\sin(\theta\omega_o) + \omega_o\cos(\theta\omega_o)}{\omega_o\left(\omega_o^2 + 1\right)},$$ (A16)

and

$$Y_I = -k_{po}\frac{\sin(\theta\omega_o) + \omega_o\cos(\theta\omega_o)}{\omega_o^2 + 1} - \left(k_{io} - k_{do}\omega^2\right)\frac{\cos(\theta\omega_o) - \omega_o\sin(\theta\omega_o)}{\omega_o\left(\omega_o^2 + 1\right)}.$$ (A17)

Note that the real and imaginary parts are both linear combinations of k_{po}, k_{io}, and k_{do}. The Nyquist plot of the loop transfer function should pass through the selected point, which is denoted as,

$$x_o = -\cos(\varphi_m) - i\sin(\varphi_m),$$ (A18)

and the corresponding gain crossover frequency is ω_{gco}.

By equaling Equation (A15) and Equation (A18), we can obtain,

$$\begin{cases} k_{po}\frac{\theta(\theta\cos(a) - a\sin(a))}{a^2 + \theta^2} - \left(k_{io}\theta^2 - k_{do}a^2\right)\frac{\theta\sin(a) + a\cos(a)}{a(a^2 + \theta^2)} = -\cos(\varphi_m) \\ -k_{po}\frac{\theta(\theta\sin(a) + a\cos(a))}{a^2 + \theta^2} - \left(k_{io}\theta^2 - k_{do}a^2\right)\frac{\theta\cos(a) - a\sin(a)}{a(a^2 + \theta^2)} = -\sin(\varphi_m) \end{cases},$$ (A19)

where a dimensionless parameter is used as $a = \omega_o\theta$ to simplify the formula derivation.

By a simple transformation, the controller parameters can be obtained as follows,

$$\begin{cases} k_{po} = \frac{1}{\theta}a\sin(\varphi_m + a) - \cos(\varphi_m + a) \\ \left(k_{io}\theta^2 - k_{do}a^2\right) = a\theta\sin(\varphi_m + a) + a^2\cos(\varphi_m + a) \end{cases}.$$ (A20)

If k_{io} is fixed, the integral time of the PID controller is,

$$\frac{k_{po}}{k_{io}\theta} = \frac{T_{io}}{\theta} = \frac{a\sin(\varphi_m + a) - \theta\cos(\varphi_m + a)}{a\theta\sin(\varphi_m + a) + a^2\cos(\varphi_m + a) + k_{do}a^2}.$$ (A21)

Obviously, Equations (A20) and (A21) offer an elegant and simple tuning formula, which will be applied to the PID tuning directly in the next section.

From Equation (A20), the expression of k_{io} can be obtained as follows,

$$k_{io} = \frac{a\theta\sin(\varphi_m + a) + a^2\cos(\varphi_m + a)}{\theta^2} + \frac{k_{do}a^2}{\theta^2}.$$ (A22)

where k_{io} is determined by three parts from Equation (A22). k_{io} is mainly determined by $a^2\cos(\varphi_m + a)$ for lag-dominant processes (large θ) and mainly determined by $a\theta\sin(\varphi_m + a)$ for delay-dominant processes (small θ) with a given k_{do}.

Here, the **Theorem A1** about stability regions are also given directly as follows.

Theorem A1. *The range of k_{po} for the given FOPDT plant in Equation (A12) can be stabilized with a PID controller is given by*

$$-1 < k_{po} < [\theta a_1\sin(a_1) - \cos(a_1)],$$ (A23)

where a_1 is the root of the following equation,

$$\tan(a_1) = -\frac{1}{1 + \theta}a_1,$$ (A24)

and a_1 is in the interval of $\left(\frac{\pi}{2}, \pi\right)$.

For a given k_{po} locating in the range of Equation (A24) and a given k_{do}, the range of k_{io} guaranteeing the stability of the closed-loop system is given by

$$0 \le k_{io} < \max\left\{\frac{\alpha}{\theta}\left[\sin(\alpha) + \frac{1}{\theta}\alpha\cos(\alpha)\right] + \frac{k_{do}\alpha^2}{\theta^2}\right\}, \tag{A25}$$

where the maximum value of α is the root of the following equation,

$$k_{po} - \frac{1}{\theta}\alpha\sin(\alpha) + \cos(\alpha) = 0, \tag{A26}$$

and α is in the interval of $(0, a_1)$.

Note that the **Theorem A1** is equivalent to the **Theorem 1** and the **Theorem 1** can be obtained by the **Theorem A1** when we substitute Kk_p, KTk_i, $k_d K/T$, and L/T for k_{po}, k_{io}, k_{do}, and θ, respectively. The proof is omitted here considering that the proof is similar with that of the **Theorem 1**.

Besides, the deductions about the PID tuning with constraints on relative delay margin is also carried out based on the time scaling and dimensionless variables.

The loop transfer function with the process model in Equation (A12) and the feedback controller in Equation (A13) can be obtained,

$$G_{Lo}(s_o) = \left[\frac{1}{\theta}a\sin(\varphi_m + a) - \cos(\varphi_m + a) + \frac{a\sin(\varphi_m+a)+\frac{1}{\theta}a^2\cos(\varphi_m+a)}{s_o} + \frac{k_{do}a^2}{\theta s_o} + \frac{k_{do}}{\theta}s_o\right]\frac{1}{1+\frac{1}{\theta}s_o}e^{-s_o}. \tag{A27}$$

To better measure the lag/delay ratio for the process model, a normalized time delay is defined as [34],

$$\tau = \frac{\theta}{\theta + 1}, \tag{A28}$$

where the range of τ is $[0, 1)$. A small τ means a lag-dominant process and a large τ means a delay-dominant process. The tuning of the PID controller with the purpose of obtaining the optimal disturbance rejection ability is analyzed as follows.

As the analysis above and Section 2.2, the PID tuning with constraints on the relative delay margin can be formulated as,

$$\begin{cases} \max \quad \dfrac{a\theta\sin(\varphi_m+a)+a^2\cos(\varphi_m+a)}{\theta^2} + \dfrac{k_{do}a^2}{\theta^2} \\ \text{s.t.} \quad R_{dm} = \dfrac{\varphi_m}{a} = r_{dm} \text{ and a given } k_d, \end{cases}$$

where the objective function is a scaled integral gain in terms of φ_m, a, and k_{do}. r_{dm} is the representative of a desired robustness level and k_{do} is the desired value of the derivative gain. To solve the objective function, the derivative function with respect to a is obtained as follows,

$$\frac{d}{da}\left[\frac{a\theta\sin(a(r_{dm}+1))+a^2\cos(a(r_{dm}+1))}{\theta^2} + \frac{k_{do}a^2}{\theta^2}\right] = 0, \tag{A29}$$

which can be further transformed to an algebraic equation,

$$\begin{aligned}[\sin(a(r_{dm}+1)) &+ a\cos(a(r_{dm}+1))(r_{dm}+1) \\ &+ \tfrac{2a\cos(a(r_{dm}+1))}{\theta} - \tfrac{a^2\sin(a(r_{dm}+1))(r_{dm}+1)}{\theta}\Big] + \tfrac{2k_{do}a}{\theta} = 0\end{aligned} \tag{A30}$$

where a is in the range of $(0, a_1)$, and Equation (A30) can be solved numerically.

Then we can summarize the design procedure based on the discussion above as follows:

(1)　The approximate FOPDT model (K, T, and L) is obtained by various approximation methods and θ in Equation (A12) can be obtained

(2) k_{do} and a desired robustness level r_{dm} are fixed. a can be obtained by solving Equation (A26).

(3) k_{po} and k_{io} are calculated by Equation (A20). The values of k_p, k_i, and k_d can be obtained. Adjust the prefilter parameters (b and c) manually to obtain the satisfactory tracking performance.

Appendix C

The proposed design method focuses on the response to input disturbance by maximizing k_i, which is the primary concern. However, it is also important to have good response to the set-point. The transfer function from the set-point to the output can be given by

$$\frac{Y(s)}{R(s)} = \frac{cT_iT_ds^2 + bT_is + 1}{T_iT_ds^2 + T_is + 1} \frac{G_c(s)G_p(s)}{1 + G_c(s)G_p(s)} = G_{ry}(s). \tag{A31}$$

In order to have a small overshoot in set-point response, set-point weighting factors b and c should be determined so that $M_{sp} = \max_{\omega} |G_{ry}(i\omega)|$ is close to one [11]. It follows from Equation (A31) that $M_{sp} \leq M_p$ when $0 \leq b \leq 1$ and $0 \leq c \leq 1$ [8], where M_p is defined by

$$M_p = \max_{\omega} |P(i\omega)| = \max_{\omega} \left| \frac{G_c(i\omega)G_p(i\omega)}{1 + G_c(i\omega)G_p(i\omega)} \right|. \tag{A32}$$

Now the influence of different b and c on the tracking performance in frequency-domain is analyzed by a simulation. Still consider Example 1, and the response of $G_{ry}(s)$ in frequency-domain with different b and c can be obtained with unchanged other parameters as shown in Figure A1. The maximum value of $|G_{ry}(i\omega)|$ is larger than one when $b > 1$ or $c > 1$. When $b = 1$ and $c = 1$, the response of $G_{ry}(s)$ is same with that of $P(s)$ because $F(s) = 1$. Therefore, the recommended ranges of b and c are both $[0, 1]$ as depicted in [8].

Note that different b and c locating in the range $[0, 1]$ can result in different tracking performance as shown in Figures A2 and A3. The values of b and c have no influence on the disturbance rejection performance but have obvious influence on the tracking performance. Note that b and c should be adjusted manually for the proposed DRO-PID, and the recommended parameters in Table 1 can be used directly which are obtained based on many simulation results.
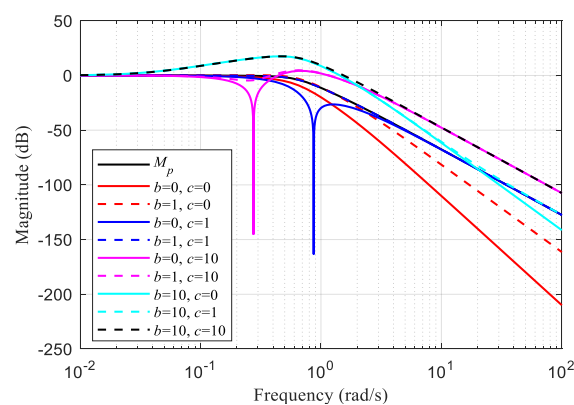

**Figure A1.** The response of $G_{sp}(s)$ in frequency-domain with different b and c.
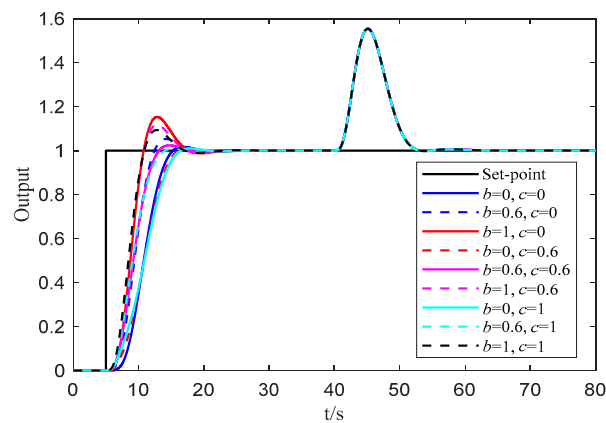
**Figure A2.** The output of tracking performance with different *b* and *c*.
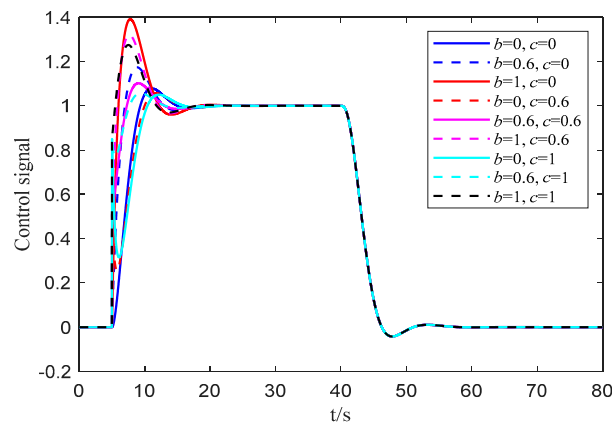
Figure A3. The control signal of tracking performance with different *b* and *c*.

References

1. Åström, K.J.; Panganamala, R.K. Control: A perspective. *Automatica* **2014**, *50*, 3–43. [CrossRef]
2. Wu, Z.L.; Li, D.H.; Xue, Y.; Chen, Y.Q. Gain Scheduling Design Based on Active Disturbance Rejection Control for Thermal Power Plant under Full Operating Conditions. *Energy* **2019**, *185*, 744–762. [CrossRef]
3. Qin, S.J.; Badgwell, T.A. A survey of industrial model predictive control technology. *Control Eng. Pract.* **2003**, *11*, 733–764. [CrossRef]
4. Li, H.; Shi, P.; Yao, D.; Wu, L. Observer-based adaptive sliding mode control for nonlinear Markovian jump systems. *Automatica* **2016**, *64*, 133–142. [CrossRef]
5. Zhao, C.; Guo, L. PID controller design for second order nonlinear uncertain systems. *Sci. China Inf. Sci.* **2017**, *60*, 022201. [CrossRef]
6. Skogestad, S. Simple analytic rules for model reduction and PID controller tuning. *J. Process Control* **2003**, *13*, 291–309. [CrossRef]
7. Ziegler, J.G.; Nichols, N.B. Optimum settings for automatic controllers. *Trans. ASME* **1942**, *64*, 759–765. [CrossRef]
8. Åström, K.J.; Tore, H. *Advanced PID Control*; The Instrumentation, Systems, and Automation Society Press: Research Triangle Park, NC, USA, 2006.
9. Åström, K.J.; Hägglund, T. Automatic tuning of simple regulators with specifications on phase and amplitude margins. *Automatica* **1984**, *20*, 645–651. [CrossRef]
10. Ogata, K. *Modern Control Engineering*; Prentice Hall: Upper Saddle River, NJ, USA, 2002; Volume 4.
11. Åström, K.J.; Panagopoulos, H.; Hägglund, T. Design of PI controllers based on non-convex optimization. *Automatica* **1998**, *34*, 585–601. [CrossRef]
12. O'Dwyer, A. *Handbook of PI and PID Controller Tuning Rules*; Imperial College Press: London, UK, 2009.

13. Hägglund, T.; Åström, K.J. Revisiting the Ziegler-Nichols tuning rules for PI control. *Asian J. Control* **2002**, *4*, 364–380. [CrossRef]

14. Wang, X.; Yan, X.; Li, D.; Sun, L. An Approach for Setting Parameters for Two-Degree-of-Freedom PID Controllers. *Algorithms* **2018**, *11*, 48. [CrossRef]

15. Sundaramoorthy, S.; Ramasamy, M. Tuning Optimal Proportional–Integral–Derivative Controllers for Desired Closed-Loop Response Using the Method of Moments. *Ind. Eng. Chem. Res.* **2014**, *53*, 17403–17418. [CrossRef]

16. Srivastava, S.; Pandit, V.S. A 2-Dof LQR based PID controller for integrating processes considering robustness/performance tradeoff. *ISA Trans.* **2017**, *71*, 426–439. [CrossRef] [PubMed]

17. Wang, C.F.; Li, D.H. Decentralized PID controllers based on probabilistic robustness. *J. Dyn. Syst. Meas. Control* **2011**, *133*, 061015. [CrossRef]

18. Begum, K.G.; Rao, A.S.; Radhakrishnan, T.K. Enhanced IMC based PID controller design for non-minimum phase (NMP) integrating processes with time delays. *ISA Trans.* **2017**, *68*, 223–234. [CrossRef]

19. Lu, K.; Zhou, W.; Zeng, G.; Du, W. Design of PID controller based on a self-adaptive state-space predictive functional control using extremal optimization method. *J. Frankl. Inst.* **2018**, *355*, 2197–2220. [CrossRef]

20. Wang, Y.; Rajamani, R.; Zemouche, A. A quadratic matrix inequality based PID controller design for LPV systems. *Syst. Control Lett.* **2019**, *126*, 67–76. [CrossRef]

21. Verma, B.; Padhy, P.K. Indirect IMC-PID controller design. *IET Control Theory Appl.* **2018**, *13*, 297–305. [CrossRef]

22. Wcislik, M.; Laskawski, M. Tuning methods of the PI and PID controllers parameters. U.S. Patent Application No. EP 2 715 458 B1, 20 March 2014.

23. Laskawski, M.; Wcislik, M. Sampling rate impact on the tuning of PID controller parameters. *Int. J. Electron. Telecommun.* **2016**, *62*, 43–48. [CrossRef]

24. Laskawski, M.; Wcislik, M. Influence of sampling on the tuning of PID controller parameter. In Proceedings of the 13th IFAC and IEEE Conference on Programmable Devices and Embedded Systems PDES 2015, Cracow, Poland, 3–15 May 2015; pp. 441–446.

25. Li, D.H.; Gao, F.; Xue, Y.; Lu, C. Optimization of decentralized PI/PID controllers based on genetic algorithm. *Asian J. Control* **2007**, *9*, 306–316. [CrossRef]

26. Killingsworth, N.J.; Krstic, M. PID tuning using extremum seeking: Online, model-free performance optimization. *IEEE Control Syst. Mag.* **2006**, *26*, 70–79.

27. Wu, Z.L.; Li, D.H.; Wang, L. Control of the superheated steam temperature: A comparison study between PID and fractional order PID controller. In Proceedings of the 35th Chinese Control Conference (CCC), Chengdu, China, 27–29 July 2016; pp. 10521–10526.

28. Han, J.; Wang, P.; Yang, X. Tuning of PID controller based on fruit fly optimization algorithm. In Proceedings of the 2012 IEEE International Conference on Mechatronics and Automation, Chengdu, China, 5–8 August 2012; pp. 409–413.

29. Fang, J.A.; Zheng, D.; Ren, Z. Computation of stabilizing PI and PID controllers by using Kronecker summation method. *Energy Convers. Manag.* **2009**, *50*, 1821–1827. [CrossRef]

30. Mercader, P.; Åström, K.J.; Banos, A.; Hägglund, T. Robust PID design based on QFT and convex–concave optimization. *IEEE Trans. Control Syst. Technol.* **2017**, *25*, 441–452. [CrossRef]

31. Hohenbichler, N. All stabilizing PID controllers for time delay systems. *Automatica* **2009**, *45*, 2678–2684. [CrossRef]

32. Ma, D.; Chen, J. Delay margin of low-order systems achievable by PID controllers. *IEEE Trans. Autom. Control* **2018**, *64*, 1958–1973. [CrossRef]

33. Zhou, Y.; Wang, D. An improved coordinated control technology for coal-fired boiler-turbine plant based on flexible steam extraction system. *Appl. Therm. Eng.* **2017**, *125*, 1047–1060. [CrossRef]

34. Sun, L.; Li, D.H.; Lee, K.Y. Optimal disturbance rejection for PI controller with constraints on relative delay margin. *ISA Trans.* **2016**, *63*, 103–111. [CrossRef] [PubMed]

35. Liu, Q.; Liu, M.; Jin, Q.B.; Liu, Y. Design of DOB-Based Control System in the Presence of Uncertain Delays for Low-Order Processes. *IEEE Trans. Control Syst. Technol.* **2018**. [CrossRef]

36. Sun, L.; Li, D.; Hu, K.; Lee, K.Y.; Pan, F. On tuning and practical implementation of active disturbance rejection controller: A case study from a regenerative heater in a 1000 MW power plant. *Ind. Eng. Chem. Res.* **2016**, *55*, 6686–6695. [CrossRef]

37. Åström, K.J.; Panagopoulos, H.; Hägglund, T. Design of PID controllers based on constrained optimization. *IEEE Proc. Control Theory Appl.* **2002**, *149*, 32–40.

38. Jin, Q.B.; Liu, Q.; Wang, Q.; Li, S.N.; Wang, Z. IMC–PID design: Analytical optimization for performance/robustness tradeoff tuning for servo/regulation mode. *Asian J. Control* **2014**, *16*, 1252–1261. [CrossRef]

39. Garrido, J.; Ruz, M.; Morilla, F.; Vázquez, F. Interactive Tool for Frequency Domain Tuning of PID Controllers. *Processes* **2018**, *6*, 197. [CrossRef]

40. Wang, L. *From Plant Data to Process Control: Ideas for Process Identification and PID Design*; CRC Press: Boca Raton, FL, USA, 2014.

41. Laskawski, M.; Wcislik, M. New optimal settings of PI and PID controllers for the first-order inertia and dead time plant. In Proceedings of the 2017 18th International Scientific Conference on Electric Power Engineering (EPE), Ostrava, Czech Republic, 17–19 May 2017; pp. 1–6.

42. Srivastava, S.; Pandit, V.S. A PI/PID controller for time delay systems with desired closed loop time response and guaranteed gain and phase margins. *J. Process Control* **2016**, *37*, 70–77. [CrossRef]

43. Silva, G.J.; Datta, A.; Bhattacharyya, S.P. New results on the synthesis of PID controllers. *IEEE Trans. Autom. Control* **2002**, *47*, 241–252. [CrossRef]

44. Xue, D.Y. *Computer Aided Control Systems Design Using MATLAB Language*; Tsinghua University: Beijing, China, 2006.